REPORT DOCUMENTATION PAGE

Form Approved OMB NO. 0704-0188

1. REPORT DATE (DD-MM-YYYY)	2. REPORT TYPE	3. DATES COVERED (From - To)
25-02-2020	Final Report	1-Jun-2015 - 31-May-2018

4. TITLE AND SUBTITLE

Final Report: Determination of Oxygen and Hydrogen Mass Transfer Coefficients in PEMFC GDE and Their Separation into Gas and Electrolyte Contributions

5a. CONTRACT NUMBER
W911NF-15-1-0188

5b. GRANT NUMBER

5c. PROGRAM ELEMENT NUMBER
611102

6. AUTHORS

5d. PROJECT NUMBER

5e. TASK NUMBER

5f. WORK UNIT NUMBER

7. PERFORMING ORGANIZATION NAMES AND ADDRESSES

University of Hawaii - Research Services
Office of Research Services
2440 Campus Road, Box 368
Honolulu, HI 96822 -2234

8. PERFORMING ORGANIZATION REPORT NUMBER

9. SPONSORING/MONITORING AGENCY NAME(S) AND ADDRESS (ES)

U.S. Army Research Office
P.O. Box 12211
Research Triangle Park, NC 27709-2211

10. SPONSOR/MONITOR'S ACRONYM(S)
ARO

11. SPONSOR/MONITOR'S REPORT NUMBER(S)
65941-CH-H.10

12. DISTRIBUTION AVAILIBILITY STATEMENT

Approved for public release; distribution is unlimited.

13. SUPPLEMENTARY NOTES

The views, opinions and/or findings contained in this report are those of the author(s) and should not contrued as an official Department of the Army position, policy or decision, unless so designated by other documentation.

14. ABSTRACT

15. SUBJECT TERMS

16. SECURITY CLASSIFICATION OF:			17. LIMITATION OF ABSTRACT	15. NUMBER OF PAGES	19a. NAME OF RESPONSIBLE PERSON
a. REPORT	b. ABSTRACT	c. THIS PAGE			Tatyana Reshetenko
UU	UU	UU	UU		19b. TELEPHONE NUMBER: 808-593-1714

Standard Form 298 (Rev 8/98)
Prescribed by ANSI Std. Z39.18

RPPR Final Report
as of 26-Feb-2020

Agency Code:

Proposal Number: 65941CHH **Agreement Number: W911NF-15-1-0188**
INVESTIGATOR(S):

Name: Tatyana V. Reshetenko
Email: tatyanar@hawaii.edu
Phone Number: 8085931714
Principal: Y

Organization: **University of Hawaii - Research Services**
Address: Office of Research Services, Honolulu, HI 968222234
Country: USA
DUNS Number: 965088057 EIN: 996000354

Report Date: 29-Feb-2016 Date Received: 25-Feb-2020
Final Report for Period Beginning 01-Jun-2015 and Ending 31-May-2018

Title: Determination of Oxygen and Hydrogen Mass Transfer Coefficients in PEMFC GDE and Their Separation into Gas and Electrolyte Contributions
Begin Performance Period: 01-Jun-2015 **End Performance Period:** 30-Nov-2019
Report Term: 0-Other

Submitted By: Tatyana Reshetenko Email: tatyanar@hawaii.edu
Phone: (808) 593-1714

Distribution Statement: 1-Approved for public release; distribution is unlimited.

STEM Degrees: **STEM Participants:**

Major Goals: Determination of oxygen and hydrogen mass transfer coefficients in PEMFC GDE and their separation into gas and electrolyte contributions

Major goals

Task 1. Method validation
1.1. Demonstrate the method reproducibility.
1.2. Identify mass transport processes responsible for the impact of the microporous layer (gas phase transport) on the oxygen mass transfer coefficient originally assigned to the ionomer (solid phase transport).
1.3. Compare the oxygen mass transport coefficients obtained using the limiting current density distribution approach by comparing them to those extracted from electrochemical impedance spectroscopy (EIS) data.

Task 2. Method development
2.1. Simplify the mass transfer coefficient separation method by decreasing the number of gaseous diluents.
2.2. Extend the applicability range of the method to lower current densities by modifying the current distribution model with a mixed kinetic and mass transfer control dependent local current.
2.3. Investigate the impact of operating conditions (pressure, gas humidity) on mass transport mechanisms at the proton exchange membrane fuel cell (PEMFC) electrodes.
2.4. Study the effects of ionomer loading and thickness on the oxygen mass transfer coefficients to clarify differences between nano-structured thin film and ionomer ink catalyst layers.
2.5. Apply the method to the anode and determine hydrogen mass transport processes.

Task 3. Outreach
3.1. Disseminate critical data, findings, interpretations and models to inform the fuel cell community about the new method to separate reactant mass transfer coefficients into their constitutive elements.

Accomplishments: Accomplishments
1. Method validation
1.1. The validity of the method was demonstrated and proven using commercially relevant flow field design developed by Nuvera Fuel Cell and membrane/electrode assemblies with different electrode structures provided by Gore and 3M. Reproducibility of oxygen mass transfer coefficient determination methods was successfully demonstrated using 1) local limiting current distribution and 2) average limiting current mathematical models.

1.2. Effects of MPL in GDL on the oxygen mass transfer coefficient were studied. An increase in MPL loadings in an electrode structure decreased the gas phase molecular diffusion as well as Knudsen and film diffusion and affected performance. There is an optimal MPL content which provides desirable mass transfer properties and high performance. Moreover, the results provided an approach on further quantitative separation of different electrode components contribution to mass transfer.
1.3. Impedance models based on a physical representation of the processes in the MEAs were developed for validation of the results obtained by the proposed limiting current distribution method. The impedance modeling approach allows kinetic and transport parameters (oxygen diffusion as well as proton conductivity) to be determined on-line in operando conditions. The EIS modeling results complemented limiting current methodology.
2. Method development
2.1. Separation of the overall O2 mass transfer coefficient into the gas phase and a combination of Knudsen and film diffusion was simplified by decreasing the number of gas diluents from 9 to 3 (He, N2 and C3F8) without losing quality.
2.2. The applicability range of the model to the mixed kinetic and mass transfer control dependent local current was expanded by including Tafel and mass transfer contributions. The extended model was validated using experimental data.
2.3. Impacts of fuel cell operating conditions such as cell temperature, gas humidification and total back pressure on the oxygen mass transfer coefficients were studied in details. An increase in reagent humidification resulted in better oxygen transport in the gas phase as well as in confined pores and through films. Variation of back pressure allowed us to determine the pressure-independent component of oxygen transport and further separate Knudsen diffusion from diffusion through ionomer/water films. The developed structure-to-properties correlations provide interplay between operating conditions, oxygen transport and fuel cell performance.
2.4. Effects of ionomer in the electrode structure on the oxygen mass transfer coefficients were evaluated using NSTF MEAs from 3M and regular ionomer ink catalyst layers (Gore MEAs). A comparison of the different electrode structures showed that NSTF were characterized by the greatest kK+film value of 0.1087 vs 0.05307 m s-1 for Gore catalyst layer with close Pt loading. At the same time, NSTF electrodes demonstrated variation in km, N2 and lower value of kK, MPL compared to Gore samples, which explained the observed differences in performance.
2.5. The proposed method was successfully applied to gain knowledge on H2 mass transport processes. Optimal operating conditions were established and recommendations on the procedure were developed. The work pioneered in development and application distribution of limiting current for analyzing H2 mass transport in realistic operating condition of working electrode structures.
3. There were 11 published papers in J. Electrochem. Soc, ESC Trans., Electrochem. Commun., RCS Advances and 6 delivered presentations.

Training Opportunities: Nothing to Report

RPPR Final Report
as of 26-Feb-2020

Results Dissemination: Publications

1. T. Reshetenko, A. Kulikovsky, “Comparison of two physical models for fitting PEM fuel cell impedance spectra measured at low air flow stoichiometry”, J. Electrochem. Soc. 163 (2016) F238.
2. T. Reshetenko, A. Kulikovsky, “Variation of PEM fuel cell physical parameters with current: Impedance spectroscopy study”, J. Electrochem. Soc. 163 (2016) F1100.
3. J. St-Pierre, T.V. Reshetenko, “PEMFC reactant mass transfer coefficient measurement and separation – method extension to the mixed kinetic and mass transfer control regime”, ECS Trans. 75 (14) (2016) 63.
4. T. Reshetenko, A. Kulikovsky, “Impedance spectroscopy characterization of oxygen transport in low- and high-Pt loaded PEM fuel cells”, J. Electrochem. Soc. 164 (2017) F1633.
5. T. Reshetenko, A. Kulikovsky, “Impedance spectroscopy study of the PEM fuel cell cathode with nonuniform nafion loading”, J. Electrochem. Soc. 164 (2017) E3016.
6. T. Reshetenko, A. Kulikovsky, “Two states of the cathode catalyst layer operation in a PEM fuel cell”, J. Electrochem. Soc. 165 (2018) F821.
7. T. Reshetenko, A. Kulikovsky, “A model for extraction of spatially resolved data from impedance spectrum of a PEM fuel cell”, J. Electrochem. Soc. 165 (2018) F291.
8. T. Reshetenko, A. Kulikovsky, “On the distribution of local current density along a PEM fuel cell cathode channel”, Electrochem. Commun. 101 (2019) 35.
9. T. Reshetenko, A. Kulikovsky, “A model for local impedance: Validation of the model for local parameters recovery from a single spectrum of PEM fuel cell”, J. Electrochem. Soc. 166 (2019) F431.
10. T. Reshetenko, A. Kulikovsky, “On the origin of high frequency impedance feature in a PEM fuel cell”, J. Electrochemical Soc. 166 (2019) F1253.
11. T. Reshetenko, A. Kulikovsky, “Nafion film transport properties in a low-Pt PEM fuel cell: Impedance spectroscopy study”, RSC Advances 9 (2019) 38797.

Presentations

1. T.V. Reshetenko, K. Bethune, G. Randolf, J. St-Pierre, “Understanding spatial PEMFCs performance under different environmental and operating conditions using a segmented cell approach”, International workshop on EEWS-2015 at KAIST, December 4, 2015, Daejeon, South Korea, Keynote speaker.
2. T.V. Reshetenko, J. St-Pierre, A. Kulikovsky, “Determination and separation of PEMFC reagents mass transport coefficients by localized limiting current approach”, Gordon Research Conference-2016 (Fuel cell), August 7-12, 2016, Easton, MA, Invited speaker.
3. J. St-Pierre, T.V. Reshetenko, “PEMFC reactant mass transfer coefficient measurement and separation – method extension to the mixed kinetic and mass transfer control regime”, 230th ECS Meeting, October 2-7, 2016, Honolulu, HI, I01-2356.
4. J. St-Pierre, T. Reshetenko, “O2 mass transfer coefficient in PEMFCs – cell voltage and MEA effects”, ECS-CSE Joint Symposium on Electrochemistry of Energy & Environment, Shanghai, China, December 2-4, 2017, Paper # EC-16.
5. T.V. Reshetenko, B.L. Ben, “Effects of structural and textural properties of GDL on oxygen mass transport coefficient in PEMFC”, Gordon Research Conference-2018 (Fuel cell), Jul. 29 – Aug. 3, 2018. Smithfield, RI.
6. T.V. Reshetenko, B.L. Ben, “Analysis of mass transport phenomena in PEMFC cathode electrode: Effects of operating conditions” 236th ECS Meeting, October 13-17, 2019, Atlanta, GA, I01A-1449.

Honors and Awards: Honors and awards

1. Keynote presentation at International workshop on Energy, Environment, Water and Sustainability (EEWS) - 2015 at Korean Advanced Institute of Science and Technology (KAIST), December 4, 2015, Daejeon, South Korea.
2. Invited presentation at Gordon Research Conference-2016 (Fuel cell), August 7-12, 2016, Easton, MA.

Protocol Activity Status:

Technology Transfer: The methodology was successfully applied to Nuvera’s single cell open flow field (SCOF) design and 3M nanostructured thin film (NSTF) membrane/electrode assemblies (MEAs) to study mass transport phenomena. These results transitioned to Nuvera and 3M for further validation and use of the methodology to understand mass transport issues in PEMFCs.

PARTICIPANTS:

RPPR Final Report
as of 26-Feb-2020

Participant Type: PD/PI
Participant: Tatyana Reshetenko
Person Months Worked: 15.00 **Funding Support:**
Project Contribution:
International Collaboration:
International Travel:
National Academy Member: N
Other Collaborators:

ARTICLES:

Publication Type: Journal Article Peer Reviewed: Y **Publication Status:** 1-Published
Journal: Journal of the Electrochemical Society
Publication Identifier Type: DOI Publication Identifier: 10.1149/2.0871603jes
Volume: 163 Issue: 3 First Page #: F238
Date Submitted: 8/19/16 12:00AM Date Published:
Publication Location:
Article Title: Comparison of two physical models for fitting PEM fuel cell impedance spectra measured at a low air flow stoichiometry
Authors: Tatyana Reshetenko, Andrei Kulikovsky
Keywords: PEM fuel cell; impedance model; fitting; experiment
Abstract: Local impedance spectra of a segmented PEM fuel cell operated at an air flow stoichiometry of = 2 are measured. The local spectra are fitted with the recent 1D and quasi-2D (q2D) physical models for PEMFC impedance. The q2D model takes into account oxygen transport in the gas channel, while the 1D model ignores this transport assuming infinite stoichiometry of the air flow. Analysis of the q2D expression for the GDL impedance Zgdl at infinite stoichiometry shows that the contribution of Zgdl to the total cell impedance rapidly decays with the frequency growth. We derive an equation for the boundary frequency f(lim), above which this contribution is small. We show that the 1D model can be fitted to the high{frequency part (f > f(lim)) of a spectrum acquired at stoichiometry of 2, ignoring the low-frequency arc due to the oxygen transport in the channel. Comparison of fitting parameters resulted from the 1D and q2D models conferms this idea.
Distribution Statement: 3-Distribution authorized to U.S. Government Agencies and their contractors
Acknowledged Federal Support: **Y**

Publication Type: Journal Article Peer Reviewed: Y **Publication Status:** 1-Published
Journal: Journal of the Electrochemical Society
Publication Identifier Type: Publication Identifier:
Volume: 1.63E+002 Issue: 3.0E+000 First Page #: 0
Date Submitted: Date Published:
Publication Location:
Article Title: Comparison of Two Physical Models for Fitting PEM Fuel Cell Impedance Spectra Measured at a Low Air Flow Stoichiometry
Authors:
Keywords: PEM fuel cell; impedance model; fitting; experiment
Abstract: Local impedance spectra of a segmented PEM fuel cell operated at an air flow stoichiometry of ? = 2 are measured. The local spectra are fitted with the recent 1D and quasi–2D (q2D) physical models for PEMFC impedance. The q2D model takes into account oxygen transport in the gas channel, while the 1D model ignores this transport assuming infinite stoichiometry of the air flow. Analysis of the q2D expression for the GDL impedance Z? gdl at ? ? ?shows that the contribution of Z? gdl to the total cell impedance rapidly decays with the frequency growth. We derive an equation for the boundary frequency flim, above which this contribution is small. We show that the 1D model can be fitted to the high–frequency part (f > flim) of a spectrum acquired at ? 」 2, ignoring the low–frequency arc due to the oxyg en transport in the channel. Comparison of fitting parameters resulted from the 1D and q2D models confirms this idea.
Distribution Statement: 3-Distribution authorized to U.S. Government Agencies and their contractors
Acknowledged Federal Support:

RPPR Final Report
as of 26-Feb-2020

Publication Type: Journal Article Peer Reviewed: Y **Publication Status:** 1-Published
Journal: ECS meeting-230, PRiME-2016, I01-2356
Publication Identifier Type: Publication Identifier:
Volume: 0 Issue: 0 First Page #: 0
Date Submitted: 10/12/16 12:00AM Date Published:
Publication Location:
Article Title: PEMFC Reactant Mass Transfer Coefficient Measurement and Separation: Method Extension to the Mixed Kinetic and Mass Transfer Control Regime
Authors: Jean St-Pierre, Tatyana V. Reshetenko
Keywords: PEMFC, mass transfer coefficient, models
Abstract: Additional cost reductions are needed for proton exchange membrane fuel cells (PEMFC) to effectively compete with internal combustion engine powered vehicles. Recent trends have focused on the use of a high current density and a lower Pt catalyst loading to reduce the quantity of expensive materials. However, such strategies have led to higher mass transfer overpotentials. These performance losses are advantageously characterized by the mass transfer coefficient. Its separation into fundamental contributions will focus research efforts to improve cell performance. A separation method previously proposed was extended, which provides information for a wider cell voltage range of relevance to duty cycling operation. (The abstarct was submitted for presentation at Electrochemical Society meeting 230)
Distribution Statement: 3-Distribution authorized to U.S. Government Agencies and their contractors
Acknowledged Federal Support: **Y**

Publication Type: Journal Article Peer Reviewed: Y **Publication Status:** 1-Published
Journal: ECS Transactions
Publication Identifier Type: DOI Publication Identifier: 10.1149/07514.0063ecst
Volume: 75 Issue: 14 First Page #: 63
Date Submitted: 10/12/16 12:00AM Date Published: 7/6/16 12:54PM
Publication Location:
Article Title: PEMFC Reactant Mass Transfer Coefficient Measurement and Separation – Method Extension to the Mixed Kinetic and Mass Transfer Control Regime
Authors: Jean St-Pierre, Tatyana V. Reshetenko
Keywords: PEMFC, mass transfer coefficient, O2 diffusion
Abstract: A kinetic and mass transfer model for a proton exchange membrane fuel cell (PEMFC) current distribution was derived and validated with data obtained with a dilute oxygen stream and three diluents (5 % O2 + 95 % He, N2 or C3F8). The overall mass transfer coefficient k increased by a factor of ~2 to ~4 with a decrease in cell potential from 0.75-0.8 to 0.2 V. Mass transfer coefficients pertaining to gas phase molecular diffusion km, and, gas phase Knudsen and solid phase ionomer diffusion ke+K respectively increased by 20 % and a factor of ~2. Below 0.6 V, the km and ke+K increase is relatively smaller and is ascribed to the larger heat generation, local temperature and diffusion coefficients. The increase in km and ke+K between 0.75 and 0.6 V is relatively larger and is attributed to the development of steep oxygen and diluent concentration gradients affecting oxygen movement.
Distribution Statement: 3-Distribution authorized to U.S. Government Agencies and their contractors
Acknowledged Federal Support: **Y**

RPPR Final Report
as of 26-Feb-2020

Publication Type: Journal Article Peer Reviewed: Y **Publication Status:** 1-Published
Journal: Journal of the Electrochemical Society
Publication Identifier Type: Publication Identifier:
Volume: Issue: First Page #:
Date Submitted: 8/19/16 12:00AM Date Published: 7/6/16 1:08PM
Publication Location:
Article Title: Variation of PEM fuel cell physical parameters with current: Impedance spectroscopy study
Authors: Tatyana Reshetenko, Andrei Kulikovsky
Keywords: PEM fuel cell; impedance model; fitting; experiment
Abstract: Experimental impedance spectra of a segmented PEM fuel cell are fitted using a numerical impedance model based on the transient macrohomogeneous equations for the cathode side. Dependence of the cell transport and kinetic parameters on the current density is reported in the range from 50 to 400 mA cm-2. The largest variation (growth by an order of magnitude) exhibit the cathode catalyst layer (CCL) proton conductivity and oxygen diffusivity. Possible mechanisms behind these changes are discussed. Moreover, proton conductivity exhibits a stepwise change at the current density ~200 mA cm-2. This jump could lead to formation of current-carrying and current-free zones over the cell surface. Recent experimental data (JES, 156 B301 (2009)) show that this configuration is indeed realized in PEMFCs with the high- and low-current density zones under the channel and rib, respectively.
Distribution Statement: 3-Distribution authorized to U.S. Government Agencies and their contractors
Acknowledged Federal Support: **Y**

Publication Type: Journal Article Peer Reviewed: Y **Publication Status:** 5-Submitted
Journal: Electrochimica Acta
Publication Identifier Type: Publication Identifier:
Volume: Issue: First Page #:
Date Submitted: 7/5/16 12:00AM Date Published: 7/6/16 3:21AM
Publication Location:
Article Title: Open{circuit impedance of the cathode catalyst layer with nonuniform ionomer loading in PEM fuel cell
Authors: Tatyana Reshetenko, Andrei Kulikovsky
Keywords: PEM fuel cell impedance, modeling, oxygen transport impedance
Abstract: We report modeling and experimental study of the cathode catalyst layer (CCL) in PEM fuel cell with nonuniform ionomer loading through the layer depth. We develop analytical model for the high-frequency impedance of the CCL. Assuming that the CCL proton conductivity exponentially decays from the membrane surface, we fit the model to experimental spectra measured at the open circuit conditions. Fitting gives the characteristic scale of the proton conductivity decay, the CCL conductivity at the membrane interface and the double layer capacitance. The method provides "reference" values for the aforementioned parameters, when the amount of water in the CCL is determined solely by external humidification of the cathode stream.
Distribution Statement: 3-Distribution authorized to U.S. Government Agencies and their contractors
Acknowledged Federal Support: **Y**

RPPR Final Report
as of 26-Feb-2020

Publication Type: Journal Article Peer Reviewed: Y **Publication Status:** 1-Published
Journal: Journal of the Electrochemical Society
Publication Identifier Type: DOI Publication Identifier: 10.1149/2.0981609jes
Volume: 163 Issue: 9 First Page #: F1100
Date Submitted: 8/19/16 12:00AM Date Published: 8/19/16 3:56PM
Publication Location:
Article Title: Variation of PEM Fuel Cell Physical Parameters with Current: Impedance Spectroscopy Study
Authors: Tatyana Reshetenko, Andrei Kulikovsky
Keywords: PEM fuel cell; impedance model; fittting; experiment
Abstract: Experimental impedance spectra of a segmented PEM fuel cell are fitted using a numerical impedance model based on the transient macrohomogeneous equations for the cathode side. Dependence of the cell transport and kinetic parameters on the current density is reported in the range from 50 to 400 mA cm?2. The largest variation (growth by an order of magnitude) exhibit the cathode catalyst layer proton conductivity ?p and oxygen diffusivity. Moreover, ?p exhibits a stepwise change at the current density ~200 mA cm?2. This jump could lead to formation of current-carrying and current-free zones over the cell surface. Recent experimental data (JES 156, B301 (2009)) show that this configuration is indeed realized in PEMFCs with the high- and low-current density zones under the channel and rib, respectively.
Distribution Statement: 3-Distribution authorized to U.S. Government Agencies and their contractors
Acknowledged Federal Support: **Y**

Publication Type: Journal Article Peer Reviewed: Y **Publication Status:** 5-Submitted
Journal: Journal of the Electrochemical Society
Publication Identifier Type: Other Publication Identifier:
Volume: Issue: First Page #:
Date Submitted: 10/12/16 12:00AM Date Published: 10/13/16 1:14AM
Publication Location:
Article Title: PEMFC reactant mass transfer coefficient separation – Mixed kinetic and mass transfer control regime
Authors: Jean St-Pierre, Tatyana V. Reshetenko
Keywords: PEMFC, mass transfer coefficient
Abstract: A kinetic and mass transfer model for a proton exchange membrane fuel cell (PEMFC) current distribution was derived and validated with data obtained with a dilute oxygen stream and three diluents (5 % O2 + 95 % He, N2 or C3F8). The overall mass transfer coefficient k increased by a factor of ~2 to ~4 with a decrease in cell potential from 0.75-0.8 to 0.2 V. Mass transfer coefficients pertaining to gas phase molecular diffusion km, and, gas phase Knudsen diffusion and solid ionomer phase diffusion k(e+K) respectively increased by 20 % and a factor of ~2. Below 0.6 V, the km and k(e+K) increase is relatively smaller and is ascribed to the larger heat generation, local temperature and diffusion coefficients. The increase in km and k(e+K) between 0.75 and 0.6 V is relatively larger and is attributed to the development of steep oxygen and diluent concentration gradients facilitating oxygen movement in the lower molecular weight diluent (larger binary diffusion coefficient).
Distribution Statement: 3-Distribution authorized to U.S. Government Agencies and their contractors
Acknowledged Federal Support: **Y**

RPPR Final Report
as of 26-Feb-2020

Publication Type: Journal Article Peer Reviewed: Y **Publication Status:** 1-Published
Journal: Journal of The Electrochemical Society
Publication Identifier Type: DOI Publication Identifier: 10.1149/2.0041711jes
Volume: 164 Issue: 11 First Page #: E3016
Date Submitted: 4/6/17 12:00AM Date Published: 2/1/17 8:00PM
Publication Location:
Article Title: Impedance Spectroscopy Study of the PEM Fuel Cell Cathode with Nonuniform Nafion Loading
Authors: Tatyana Reshetenko, Andrei Kulikovsky
Keywords: PEM fuel cell impedance, modeling, cathode catalyst layer, nonuniform ionomer loading
Abstract: We report modeling and experimental study of impedance of the PEM fuel cell cathode with nonuniform ionomer loading. A physics–based model for the high–frequency impedance is developed and analytical solution for impedance is derived. Assuming that the CCL proton conductivity ?p exponentially decays from the membrane surface, we fit the model to experimental spectra of the cell measured at the open circuit conditions. Fitting gives the characteristic scale of the ?p decay, the average CCL proton conductivity and the double layer capacitance.
Distribution Statement: 3-Distribution authorized to U.S. Government Agencies and their contractors
Acknowledged Federal Support: **Y**

Publication Type: Journal Article Peer Reviewed: Y **Publication Status:** 1-Published
Journal: Journal of The Electrochemical Society
Publication Identifier Type: DOI Publication Identifier: 10.1149/2.1131714jes
Volume: 164 Issue: 14 First Page #:
Date Submitted: 3/8/18 12:00AM Date Published: 12/1/17 10:00AM
Publication Location:
Article Title: Impedance Spectroscopy Characterization of Oxygen Transport in Low– and High–Pt Loaded PEM Fuel Cells
Authors: Tatyana Reshetenko, Andrei Kulikovsky
Keywords: PEM fuel cell impedance; oxygen mass transfer coefficient, fitting
Abstract: We report fitting of the physics–based model for the cathode side impedance to the experimental spectra of low–Pt loaded (0.1/0.1mgPt cm?2) and high–Pt loaded (0.4/0.4 mgPt cm?2) PEM fuel cells measured in the range of current densities from 50 to 400 mA cm?2. Fitting allowed us to separate the oxygen diffusion coefficients in the catalyst layer Dox and in the gas–diffusion layer Db, and the respective mass transfer coefficients. In the low–Pt electrode, Dox is an order of magnitude lower, than in the high–Pt electrode; however, due to 4–fold difference in the electrode thickness, the respective mass transfer coefficients are close to each other. In both the electrodes, the oxygen diffusion and the mass transfer coefficients in the GDL are nearly the same. The ORR Tafel slope and Dox exhibit linear growth with the cell current density; both effects could be attributed to “cleaning” of Pt surface from oxides at lower cell potential.
Distribution Statement: 3-Distribution authorized to U.S. Government Agencies and their contractors
Acknowledged Federal Support: **Y**

RPPR Final Report
as of 26-Feb-2020

Publication Type: Journal Article Peer Reviewed: Y **Publication Status:** 1-Published
Journal: Journal of The Electrochemical Society
Publication Identifier Type: DOI Publication Identifier: 10.1149/2.0511805jes
Volume: 165 Issue: 5 First Page #: F291
Date Submitted: 3/27/18 12:00AM Date Published: 3/1/18 10:00AM
Publication Location:
Article Title: A Model for Extraction of Spatially Resolved Data from Impedance Spectrum of a PEM Fuel Cell
Authors: Tatyana Reshetenko, Andrei Kulikovsky
Keywords: PEM fuel cell impedance; spatial non-uniformities, fitting
Abstract: We report a novel approach to processing of impedance spectra of a PEM fuel cell. We split the cell into N virtual segments and let each segment to have its own set of transport and kinetic parameters. The impedance of a single segment is calculated using our recent physics–based impedance model; the segments are “linked” by equation for the oxygen mass balance in the cathode channel transporting the local phase and amplitude information from one segment to another. Thanks to this transport, the total cell impedance contains information on the local transport and kinetic properties of the cell. We show that fitting the model cell impedance to the experimental spectra yields the parameters of individual segments, i.e., the shape of the cell physical parameters along the cathode channel.
Distribution Statement: 3-Distribution authorized to U.S. Government Agencies and their contractors
Acknowledged Federal Support: **Y**

Publication Type: Journal Article Peer Reviewed: Y **Publication Status:** 1-Published
Journal: Journal of The Electrochemical Society
Publication Identifier Type: DOI Publication Identifier: 10.1149/2.0541810jes
Volume: 165 Issue: 10 First Page #: F821
Date Submitted: 7/25/18 12:00AM Date Published: 7/1/18 8:00PM
Publication Location:
Article Title: Two States of the Cathode Catalyst Layer Operation in a PEM Fuel Cell
Authors: Tatyana Reshetenko, Andrei Kulikovsky
Keywords: PEM fuel cell impedance; spatial non-uniformities, local flooding
Abstract: We measure impedance of a standard Pt/C–based PEM fuel cell for a series of current densities from 50 to 400 mA cm?2. Using our recent model for extraction of spatially–resolved data from impedance spectra, we plot the dependence of the oxygen diffusion coefficient Dox in the cathode catalyst layer (CCL) and Db in the gas–diffusion layer (GDL) on the distance along the cathode channel. While the GDL oxygen diffusivity is fairly uniform over the cell active area, the shape of Dox indicates that the cell is separated into two domains with high and low water contents in the CCL. We attribute this effect to the positive feedback loop between the rates of oxygen transport and liquid water evaporation in the CCL, leading to local CCL flooding.
Distribution Statement: 3-Distribution authorized to U.S. Government Agencies and their contractors
Acknowledged Federal Support: **Y**

Publication Type: Journal Article Peer Reviewed: Y **Publication Status:** 1-Published
Journal: Electrochemistry Communications
Publication Identifier Type: DOI Publication Identifier: 10.1016/j.elecom.2019.02.005
Volume: 101 Issue: First Page #: 35
Date Submitted: 3/9/19 12:00AM Date Published: 4/1/19 12:00AM
Publication Location:
Article Title: On the distribution of local current density along a PEM fuel cell cathode channel
Authors: Tatyana Reshetenko, Andrei Kulikovsky
Keywords: PEM fuel cell, Local current distribution, Modeling, Experiment
Abstract: We report analysis of a recent model for local current density distribution along the air channel in a PEM fuel cell. Analytical solution for the case of small cell ohmic resistivity is obtained. An algorithm for numerical solution of the model equations is developed for practically important case when the cell polarization curve and ohmic resistivity are known. Good agreement between the calculated and experimental shapes of the local current density is demonstrated. Cell ohmic resisitivty greatly homogenizes the distribution of local current. A Python code for local current calculation is available for download.
Distribution Statement: 3-Distribution authorized to U.S. Government Agencies and their contractors
Acknowledged Federal Support: **Y**

Publication Type: Journal Article Peer Reviewed: Y **Publication Status:** 1-Published
Journal: Journal of The Electrochemical Society
Publication Identifier Type: DOI Publication Identifier: 10.1149/2.1241906jes
Volume: 166 Issue: 6 First Page #: F431
Date Submitted: 8/29/19 12:00AM Date Published: 4/1/19 10:00AM
Publication Location:
Article Title: A Model for Local Impedance: Validation of the Model for Local Parameters Recovery from a Single Spectrum of PEM Fuel Cell
Authors: Tatyana Reshetenko, Andrei Kulikovsky
Keywords: PEM fuel cell; impedance model; kinetic and transport parameters
Abstract: A physics–based numerical model for fitting local impedance spectra (local impedance model, LIM) of the segmented PEM fuel cell is developed and used to validate our recent model for recovery of local parameters from a single spectrum of the whole cell (cell impedance model, CIM). Shapes of the local parameters along the cathode channel resulting from the two models are compared. Overall, the CIM quite satisfactorily describes the cell local parameters provided that the oxygen transport impedance in the channel is not small as compared to other impedances in the cell.
Distribution Statement: 3-Distribution authorized to U.S. Government Agencies and their contractors
Acknowledged Federal Support: **Y**

CONFERENCE PAPERS:

Publication Type: Conference Paper or Presentation **Publication Status:** 1-Published
Conference Name: International workshop on Enerfy, Enviroment, Water and Sustainability - 2015
Date Received: 29-Aug-2019 Conference Date: 05-Dec-2015 Date Published: 05-Dec-2019
Conference Location: Daejeon, Korea
Paper Title: Understanding spatial PEMFCs performance under different environmental and operating conditions using a segmented cell approach
Authors: Tatyana V. Reshetenko, Keith Bethune, Günter Randolf, Jean St-Pierre
Acknowledged Federal Support: **Y**

Publication Type: Conference Paper or Presentation **Publication Status:** 1-Published
Conference Name: International workshop on Energy, Environment, Water and Sustainability-2015
Date Received: 30-Aug-2019 Conference Date: 05-Dec-2015 Date Published: 05-Dec-2015
Conference Location: Daejeon, Korea
Paper Title: Understanding spatial PEMFCs performance under different environmental and operating conditions using a segmented cell approach
Authors: Tatyana V. Reshetenko, Keith Bethune, Günter Randolf, Jean St-Pierre
Acknowledged Federal Support: **Y**

Publication Type: Conference Paper or Presentation **Publication Status:** 1-Published
Conference Name: Gordon Research Conference-2016 (Fuel cell)
Date Received: 30-Aug-2019 Conference Date: 08-Aug-2016 Date Published:
Conference Location: Easton, MA, USA
Paper Title: Determination and separation of PEMFC reagents mass transport coefficients by localized limiting current approach
Authors: T.V. Reshetenko, J. St-Pierre, A. Kulikovsky
Acknowledged Federal Support: **Y**

RPPR Final Report
as of 26-Feb-2020

Publication Type: Conference Paper or Presentation **Publication Status:** 1-Published
Conference Name: ECS meeting-230
Date Received: 30-Aug-2019 Conference Date: 03-Oct-2016 Date Published: 03-Oct-2016
Conference Location: Honolulu, HI, USA
Paper Title: PEMFC reactant mass transfer coefficient measurement and separation – method extension to the mixed kinetic and mass transfer control regime
Authors: J. St-Pierre, T.V. Reshetenko
Acknowledged Federal Support: **Y**

Publication Type: Conference Paper or Presentation **Publication Status:** 1-Published
Conference Name: ECS-CSE Joint Symposium on Electrochemistry of Energy & Environment
Date Received: 30-Aug-2019 Conference Date: 05-Dec-2017 Date Published: 05-Dec-2017
Conference Location: Shanghai, China
Paper Title: O2 Mass Transfer Coefficient in PEMFCs – Cell Voltage and MEA Effects
Authors: J. St-Pierre, T. Reshetenko
Acknowledged Federal Support: **Y**

Publication Type: Conference Paper or Presentation **Publication Status:** 1-Published
Conference Name: Gordon Research Conference-2018 (Fuel cell)
Date Received: 30-Aug-2019 Conference Date: 30-Jul-2018 Date Published: 30-Jul-2018
Conference Location: Smithfield, RI, USA
Paper Title: Effects of structural and textural properties of GDL on oxygen mass transport coefficient in PEMFC
Authors: T.V. Reshetenko, B.L. Ben
Acknowledged Federal Support: **Y**

Publication Type: Conference Paper or Presentation **Publication Status:** 1-Published
Conference Name: ECS Meeting-236
Date Received: 30-Aug-2019 Conference Date: 14-Oct-2019 Date Published: 14-Oct-2019
Conference Location: Atlanta, GA, USA
Paper Title: Analysis of mass transport phenomena in PEMFC cathode electrode: Effects of operating conditions
Authors: T.V. Reshetenko, B.L. Ben
Acknowledged Federal Support: **Y**

Determination of oxygen and hydrogen mass transfer coefficients in PEMFC GDE and their separation into gas and electrolyte contributions

Tatyana V. Reshetenko (PI)

Abstract (200 words)

The purpose of the project was development and validation of a novel methodology on determination and separation of reactant mass transfer coefficients in heterogeneous electrode structures. The method is based on measurements of the limiting current distribution over an electrode area and utilizes operation with highly diluted reagent mixtures (~3-10 vol.% of H_2 or O_2). Variations in diluent molecular weights (from He to C_3H_8) and operating conditions allow us to separate a gas phase molecular diffusion, a Knudsen diffusion and a diffusion through ionomer/water films. The validity of the method was demonstrated and proven using commercially relevant flow field design developed by Nuvera Fuel Cell and membrane/electrode assemblies with different electrode structures provided by Gore and 3M. Effects of catalyst loading and gas diffusion layer properties on O_2/H_2 diffusion processes were studied and provided an approach on quantitative separation of different electrode components' contribution to the reagents mass transport resistance. Reactant mass transfer coefficients were determined for a wide range of operating conditions and showed an interplay between performance, operating parameters and mass transport phenomena in working heterogeneous electrode structures. Physics-based electrochemical impedance models were developed to understand kinetic and mass transport processes and complement the limiting current distribution methodology.

Determination of oxygen and hydrogen mass transfer coefficients in PEMFC GDE and their separation into gas and electrolyte contributions

Tatyana V. Reshetenko (PI)

Hawaii Natural Energy Institute
1680 East-West Road
Honolulu, HI 96822
Phone: (808) 593-1714
Email: tatyanar@hawaii.edu

ARO Program manager Dr. Robert A. Mantz
Phone: (919) 549-4309
Email: robert.a.mantz.civ@mail.mil

Contract Number 65941-CH-H
Agreement number W911NF-15-1-0188

Subcontractors
Dr. Olga Polevaya
Nuvera Fuel Cell, LLC; 129 Concord Road, Building 1, Billerica, MA, 01821, USA

Collaborators
Dr. Andrei Kulikovsky
Institute of Energy and Climate Research, Research Center "Juelich", D-52425 Juelich, Germany
Dr. Andy Steinbach
3M, Corporate R&D, 3M Center, 201-2N-19, St. Paul, MN 55144-1000, USA

Project Start Date: June 1, 2015

Project End Date: November 30, 2019

Table of contents

1. Statement of the problem studied

High-power generation of electrochemical conversion systems like fuel cells (proton exchange membrane fuel cells (PEMFCs)), direct liquid fuel cells) and metal/air batteries strongly depends on the mass transfer of reagents through confined and heterogeneous electrode structures. Reagent transport from a gas phase to catalyst sites occurs through molecular diffusion, Knudsen diffusion in fine pores and diffusion through thin films within a gas diffusion electrode (GDE), consisting of a gas diffusion layer (GDL) and a catalyst layer (CL). The GDL is a specifically designed porous medium that is constructed from an electrically conductive carbon macroporous substrate, e.g. a carbon paper or cloth treated by a hydrophobic agent like polytetrafluoroethylene (PTFE) to achieve the desired wettability. The GDL has a thin microporous layer (MPL) of carbon black mixed with PTFE to ensure better electrical contact and mechanical compatibility with electrode layer [1].

The type of reagent transport depends on GDE components: molecular diffusion takes place at a carbon paper, when gas molecules collide with each other, instead of pore walls. MPL and CL have similar meso- and micro-porous textures with pore sizes of 50-150 nm that favor Knudsen diffusion [2, 3]. Catalyst layer is a very complex structure consisting of catalyst agglomerates, partially covered by water and ionomer films with varied thickness (~1-10 nm). Thus, reagent mass transport in the CL proceeds through dissolution in water/ionomer and further diffusion within a film to a catalyst surface.

Specifically, PEMFCs are using air as an affordable oxidant; however, air is dilute and contains only 21% O_2 which results in mass transfer losses when operating at high-power conditions. In addition, operation of real PEMFC stacks requires high fuel efficiency which is achieved through operation with low H_2 stoichiometry and implementing H_2 recirculation or adopting dead-end anode operation. However, these strategies lead to diffusion of water and N_2 from a cathode to an anode and their accumulation at the anode flow field which affects H_2 mass transport. Thus, efficient performance of PEMFC strongly depends on mass transfer properties of flow field as well as electrode morphology and a better understanding of diffusion in a heterogeneous, three-phase electrode layer with varied texture and structure is strictly required. In order to gain this knowledge, it is crucial to have a method for allowing mass transport characteristics to be determined in realistic and in operando conditions.

In this work, we developed and validated a novel method on determination and separation of reactant mass transfer coefficient in heterogeneous electrode structure. The method is based on measurements of limiting current distributions in PEMFCs and utilizes operation at low concentrated reagent (O_2 or H_2) mixtures with different diluents (from He to C_3H_8) [4]. The method allows us to separate a gas phase molecular diffusion, a diffusion in fine pores or Knudsen diffusion and a transport through ionomer/water films. The applicability of the method was evaluated using commercial fuel cell components from Nuvera Fuel Cell, Gore and 3M. The obtained results were complemented by independent measurements and modeling of electrochemical impedance spectroscopy data. This final report highlights the most important results and puts particular emphasis on application of the method for finding H_2 mass transport parameters.

2. Overall Objectives

Task 1. Method validation

1.1. Demonstrate the method reproducibility.

1.2. Identify mass transport processes responsible for the impact of the microporous layer (gas phase transport) on the oxygen mass transfer coefficient originally assigned to the ionomer (solid phase transport).

1.3. Compare the oxygen mass transport coefficients obtained using the limiting current density distribution approach by comparing them to those extracted from electrochemical impedance spectroscopy (EIS) data.

Task 2. Method development

2.1. Simplify the mass transfer coefficient separation method by decreasing the number of gaseous diluents.

2.2. Extend the applicability range of the method to lower current densities by modifying the current distribution model with a mixed kinetic and mass transfer control dependent local current.

2.3. Investigate the impact of operating conditions (pressure, gas humidity) on mass transport mechanisms at the proton exchange membrane fuel cell (PEMFC) electrodes.

2.4. Study the effects of ionomer loading and thickness on the oxygen mass transfer coefficients to clarify differences between nano-structured thin film and ionomer ink catalyst layers.

2.5. Apply the method to the anode and determine hydrogen mass transport processes.

Task 3. Outreach

3.1. Disseminate critical data, findings, interpretations and models to inform the fuel cell community about the new method to separate reactant mass transfer coefficients into their constitutive elements.

3. Summary of the most important results

3.1. The limiting current density distribution model

The limiting current density distribution model was in details discussed in our previous publications [4, 5]. The main assumptions of the model are:

1. Unit cell has straight reactant channels,
2. Cell performance is averaged over the cross-channel direction (plug flow reactor),
3. Cell voltage is constant along the cell length,
4. Isothermal and isobaric operation,
5. Reactants are saturated with water vapor and follow the ideal gas law.

For the case of a highly dilute reactant stream the distribution of the limiting currents along flow field can be presented as:

$$i_{lim}(\tilde{x}) = \frac{nFkp_r\alpha_{O_2}^0}{RT} e^{-nFkp_r\tilde{x}/RTi_ef} \quad (1)$$

Where $\tilde{x}$ is the dimensionless position along the flow field length,
k is mass transfer coefficient,
n is the number of electrons exchanged in the electrochemical reaction,
n=4 for oxygen reduction reaction (ORR) and n=2 for hydrogen oxidation reaction (HOR),
p_r is the dry inlet reactant stream pressure (Pa),

$\alpha_{O_2}^0$ is the reactant fraction in the dry inlet reactant stream,
R is the ideal gas constant (8.3143 J mol^{-1} K^{-1}),
F is the Faraday constant (96500 C mol^{-1}),
T is the temperature (K),
i_e is the inlet reactant flow rate equivalent current density (A m^{-2}) and
f is the inert gas to reactant fraction in the dry inlet reactant stream.

The corresponding average limiting current density i_{ave} (A m^{-2}) is:

$$i_{ave} = i_e \left(1 - e^{-nFkp_r / RTi_e f}\right) \quad (2)$$

$$\ln\left(1 - \frac{i_{ave}}{i_e}\right) = \frac{-nFp_r k}{RT} \frac{1}{i_e f} \quad (3)$$

The inlet reactant flow rate equivalent current density can be expressed as:

$$i_e = \frac{nFv_{O_2}^0}{AN_m} \quad (4)$$

where $v_{O_2}^0$ is oxygen flow rate (ml s^{-1}), A is the active area of the MEA (cm^2) and N_m is the molar volume (22414 ml mol^{-1}). Alternatively, determination of the mass transport coefficient can be done with Eqs. 2 and 3 by varying the reactant flow rate ($i_e f$) and measuring i_{ave}.

3.2. Experimental details

All experiments were conducted using Hawaii Natural Energy Institute's (HNEI's) segmented cell system. This diagnostic tool enables the collection of spatially distributed electrochemical parameters such as current, voltage and impedance during a standard experiment [6]. The segmented cell setup includes cell hardware, a custom-built current transducer system and a NI PXI DAQ. For current sensing, closed loop Hall sensors from Honeywell (Model CSNN191) were used. Segment currents of up to 2 A cm^{-2} can be measured in the high current mode.

The segmented cell hardware was based on an HNEI 100 cm^2 cell design. The hardware contains a regular flow field and segmented flow field, which consists of ten cell segments forming a continuous path along ten parallel serpentine channels. Each segment has an area of 7.6 cm^2 and its own distinct current collector as well as separate GDL. The segmentation is applicable to either the anode or the cathode.

Limiting current measurements for ORR were performed using 5% O_2 diluted with various gases (He, Ne, N_2, Ar, CO_2, Kr, CF_4, SF_6 and C_3F_8) as cathode feed, while anode was supplied by pure H_2. It should be noted that the segmented cell is operated as a single fuel cell using a house-built test station. The tests were done at cell temperature of 60 and 80°C, back pressure varied from ambient to 150 kPa$_g$ (250 kPa absolute pressure). Effects of reactant humidification were evaluated at 32, 50 and 100%RH. For these experiments segmentation was applied for cathode. Polarization (IV) curves were measured with fixed reactant flow rates and under potentiostatic control of the load at a configuration typical for PEMFC testing. Details can be found in [4].

Limiting current measurements for HOR were done in H_2 pump configuration. Also, segmentation was applied for anode electrode. These tests were carried out using 10% H_2 mixture with He, Ne, N_2, Ar, CF_4 to feed anode, while cathode was supplied by pure H_2.

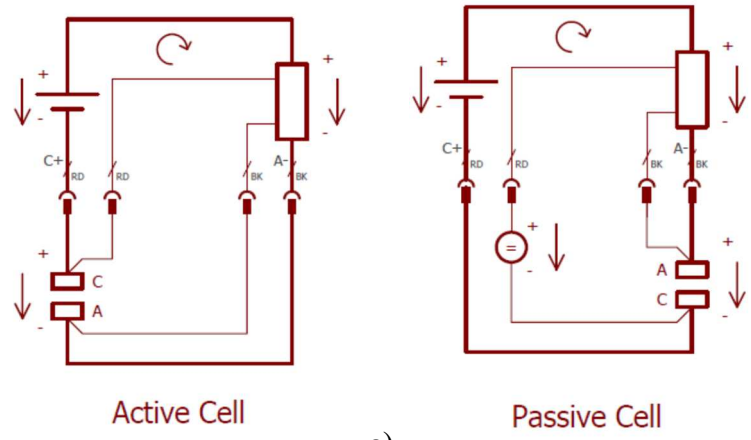

a) b)

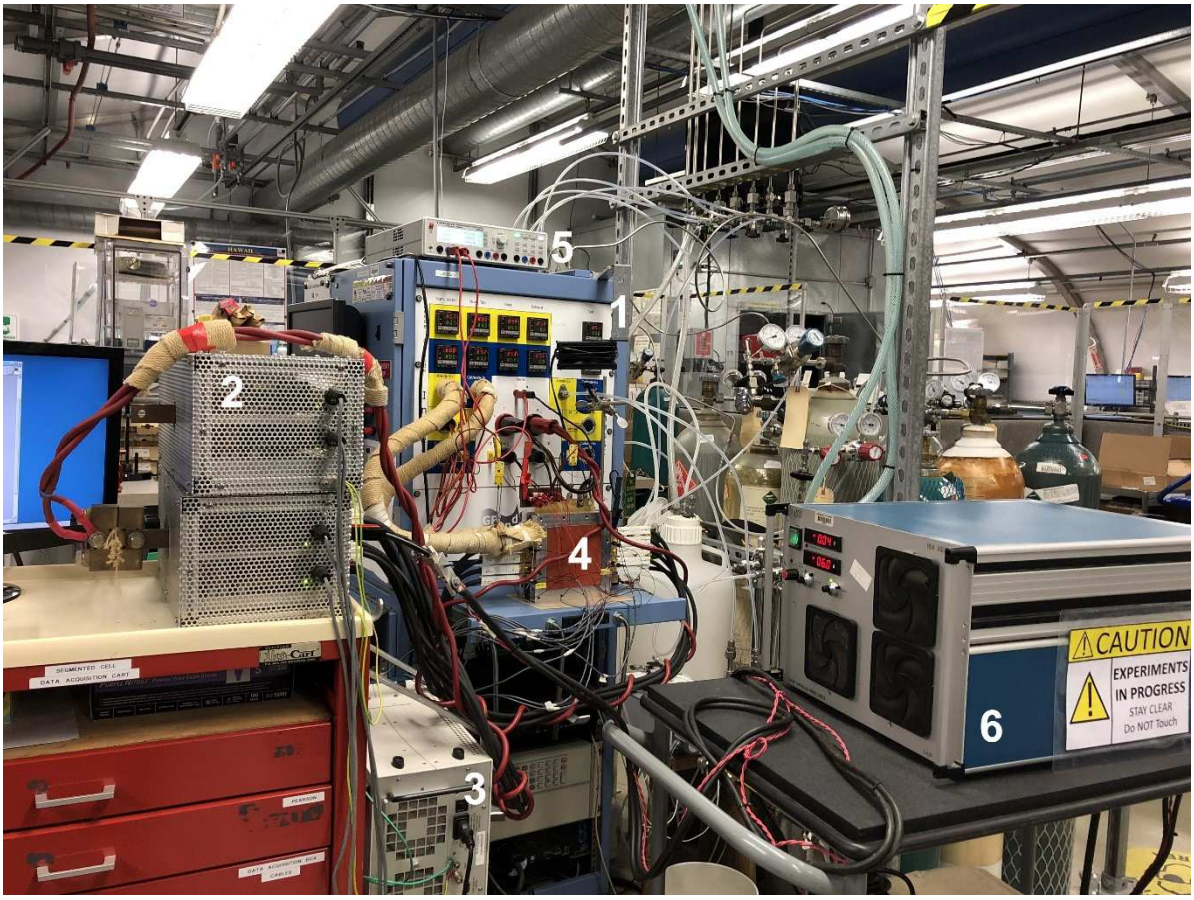

c)

Fig. 1. Wire configuration for active (a) and passive (b) setups. Segmented cell system with test station wired to additional power sources for passive operation (c): 1 – test station, 2 – custom-built current transducer system, 3 – PXI DAQ, 4 – segmented cell hardware, 5 – power supply HMP 2030 (Hameg) in voltage sensing circuit, 5 – power supply FuG added to segmented current transducer system to increase the range of detected current.

To run the cell in passive mode, which is also called a H_2 pump, it is required to change the wiring. Usually the cell and the voltage booster are in serial connection, and connected to the electronic load which serves as current regulator (Fig. 1 a). In H_2 pump mode, the voltage booster is the only active element and the cell is a consumer. That implies that it is working in a different quadrant of the

voltage-current plane and, since the current continues to flow in the same direction, the voltage is reversed. If the load is used in current controlled mode, a simple reversal of the voltage sensing cables is sufficient to avoid negative input to the load, the actual control parameter is the measured current which did not change direction. In voltage-controlled mode, however, an extra power supply (HMP 2030 Hameg) is required in anti-serial connection to the cell (Fig. 1 b). This causes the cell voltage to be subtracted from the power supply, resulting in a positive signal that decreases with increasing current, tricking the load to operate as desired. It is important that the extra power supply is very stable and that the load's set-point and reading needs to be rescaled. The new scale has a negative slope with the power supply's voltage as maximum where the cell voltage is zero.

Furthermore, we faced with the situation when currents generated by the inlet segments were out of the range of the current transducers. So, the range of the segmented cell measurement needs to be increased. This can be done by applying a reverse current through the auxiliary port, which is a wire looping through all current sensors using additional power supply unit (FuG) (Fig. 1 c). If the current is reversed, it will be subtracted from the measurement allowing for increased range and double it from 2 to 4 A cm^{-2}.

3.3. Task 1. Method validation

3.3.1. Subtask 1.1. The method reproducibility

The reproducibility was demonstrated by comparing methods based on the 1) local limiting current distribution (Eq. 1) and 2) the average limiting current (Eqs. 2, 3). Three MEAs from two batches were studied (MEA1 was from batch#1, MEA2 and 3 were from batch#2). Anode and cathode Pt loadings were 0.1 and 0.2 mg Pt cm^{-2}, respectively. 25BC was used as GDL for both electrodes.

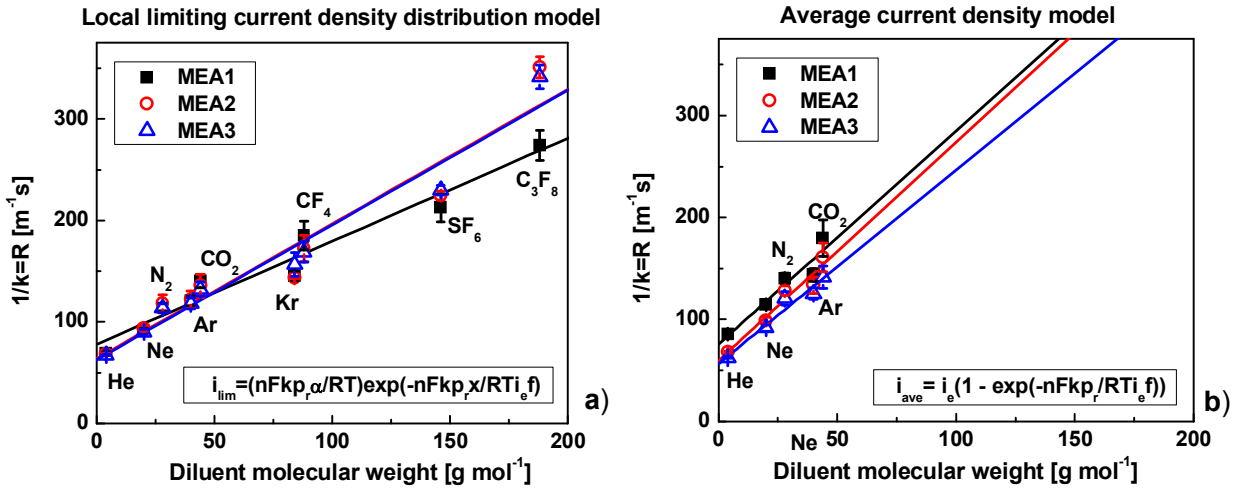

Fig. 2. Effect of the diluent molecular weight on the overall oxygen mass transport coefficient as determined by the local limiting current distribution (a) and the average limiting current (b) approaches. An/Ca: H_2/5%O_2+Diluent, 100/100RH, 150/150 kPa, 60°C.

Both approaches revealed a strong correlation between mass transfer resistance which is inverse value of mass transfer coefficient ($R=1/k$) and the diluent molecular weight (Fig. 2). The use of different gas diluents affects only mass transfer coefficients in the gas phase due to molecular diffusion (k_m)

and does not impact mass transfer coefficient in fine pores (Knudsen diffusion) and through the ionomer/water films (k_{K+film}) enabling the separation of these two contributions [4]:

$$\frac{1}{k} = \frac{1}{k_{K+film}} + \frac{1}{k_m} = \frac{1}{k_{K+film}} + bM \quad (5)$$

where M is the diluent molecular weight (mol g^{-1}).

An extrapolation to a diluent with zero molecular weight gives the O_2 mass transport coefficient due to Knudsen and film diffusions (y-axis intercept). Table 1 demonstrated the obtained mass transfer coefficients using two approached. Results showed a good reproducibility of the methods for samples from one batch (MEA2 and MEA3) as well as from different batches (MEA1 and MEA2/MEA3). Mass transfer parameters are of the same order of magnitude and in agreement with previously published results [7-11].

Table 1. Oxygen mass transfer coefficient in N_2 ($k_{m, N2}$) and through fine pores and films (k_{K+film}).

Sample	Method	k_{K+film} [m s^{-1}]	$k_{m, N2}$ [m s^{-1}]
MEA1	local average	0.01284 0.01319	0.02727 0.01561
sMEA2	local average	0.01564 0.01678	0.01855 0.01457
MEA3	local average	0.01593 0.01766	0.01972 001563

3.3.2. Subtask 1.2. Effects of MPL on O_2 mass transport

To identify the effects of MPL on PEMFC performance and oxygen mass transfer coefficient, six different GDL samples with varied MPL loadings (50 - 150%) were chosen for studies. GDLs were obtained from SGL company and were based on 25BA diffusion media with 50, 75, 100, 125 and 150% of MPL loading. A sample with 100% of MPL on 25BA is 25BC material. Textural properties of the GDLs were evaluated using mercury intrusion porosometry (MIP), while morphology was studied by SEM. Pore size distribution (PSD) of the samples are characterized by four regions, including mesopores (0.01-0.3 μm), macropores I (0.3-10 μm), macropores II (10-30 μm) and macropores III (30-500 μm) (Fig. 3 a, b; Table 2). Macropores result from carbon paper (Fig. 3 c) and mesopores originate from MPL material as can be seen from SEM image at Fig. 3 d. An increase in MPL loading led to a growth in the volume of mesopores, while the volume of macropores III decreased.

Impacts of MPL loading on O_2 mass transport and fuel cell performance were investigated using MEAs from Gore with Pt loadings of 0.1 and 0.4 mg_{Pt} cm^{-2} for anode and cathode, respectively.

Table 2 summarizes the oxygen mass transfer coefficient values. MEA1 does not have an MPL at the cathode GDL, so the obtained k_{K+film} refers to oxygen transport at the catalyst layer. Thus, we could estimate the contribution of MPL ($k_{K, MPL}$) for samples MEA2-6, since the MEAs were from the same batch and the cathode electrochemical areas (ECAs) are similar. Cumulative oxygen mass transport resistance through fine pores and films is a sum of contributions arising from the MPL and catalyst layer:

$$\frac{1}{k_{K+film}} = \frac{1}{k_{K,MPL}} + \frac{1}{k_{K+film,CL}} \quad (6)$$

We can extract mass transfer coefficient originated from Knudsen diffusion in MPL:

$$k_{K+film,CL} = k_{K+film}(MEA1) \quad (7)$$

$$k_{K,MPL} = \left(\frac{1}{k_{K+film}} - \frac{1}{k_{K+film\,(MEA1)}}\right)^{-1} \quad (8)$$

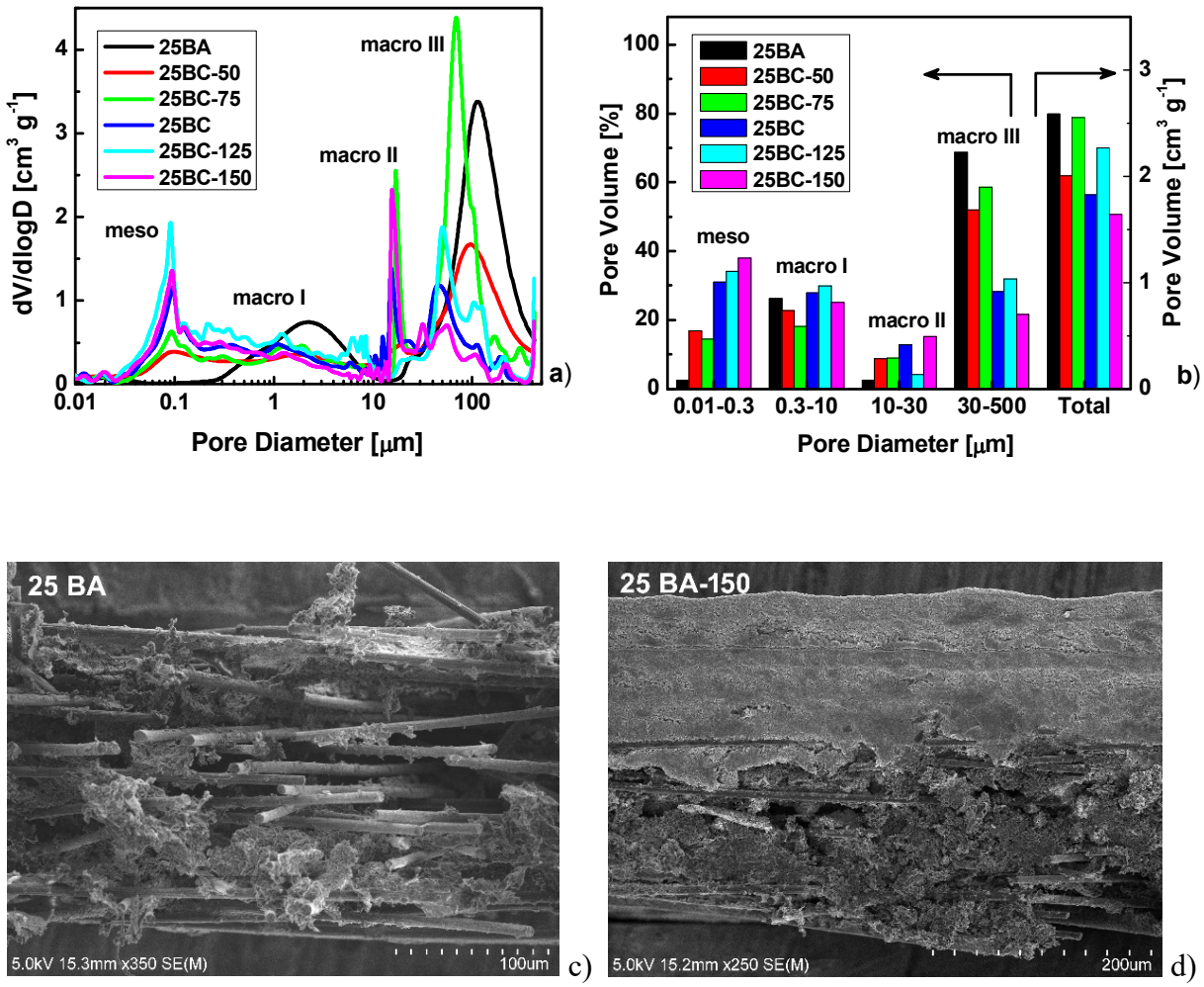

Fig. 3. Pore size distribution of GDLs (a), pore volume for regions with different pore sizes (b); SEM images of 25BA (c), 25BA-150 (150% of MPL loading) (d).

The obtained structure-to-properties correlations revealed a strong connection between GDL morphology, oxygen transfer properties and performance (Fig. 4). Clear linear relationships were found between MPL loading and textural GDL properties as well as between MPL content and *k*. An increase in MPL resulted in a growth of mesoporous volume and a decrease in macroporous volume, causing a decrease in O_2 mass transfer coefficients values. The dependence of performance from meso- and macroporous volumes goes through a maximum indicating at a trade-off between these two pore volumes.

Table 2. GDLs parameters and oxygen mass transfer coefficients in N_2 media ($k_{m,\,N2}$), cumulative value for Knudsen + films diffusion (k_{K+film}) and separate contribution arising from MPL ($k_{K,\,MPL}$). Anode/cathode: H_2/5%O_2+Diluent, 100/100% RH, 150/150 kPa, 60°C.

Sample	GDL cathode				k_{K+film} [m s^{-1}]	$k_{K,\,MPL}$ [m s^{-1}]	$k_{m,\,N2}$ [m s^{-1}]
	GDL	MPL [%]	Thickness [μm]	V_{pore} [cm^{-3} g^{-1}]			
MEA1	25BA	0	180	2.588	0.0222	-	0.0274
MEA2	25BA-50	50	190	2.007	0.0199	0.1984	0.0314
MEA3	25BA-75	75	195	2.554	0.0181	0.0984	0.0332
MEA4	25BC	100	220-230	1.824	0.0165	0.0636	0.0282
MEA5	25BA-125	125	240-250	2.271	0.0149	0.0449	0.0294
MEA6	25BA-150	150	260	1.639	0.0139	0.0374	0.0247

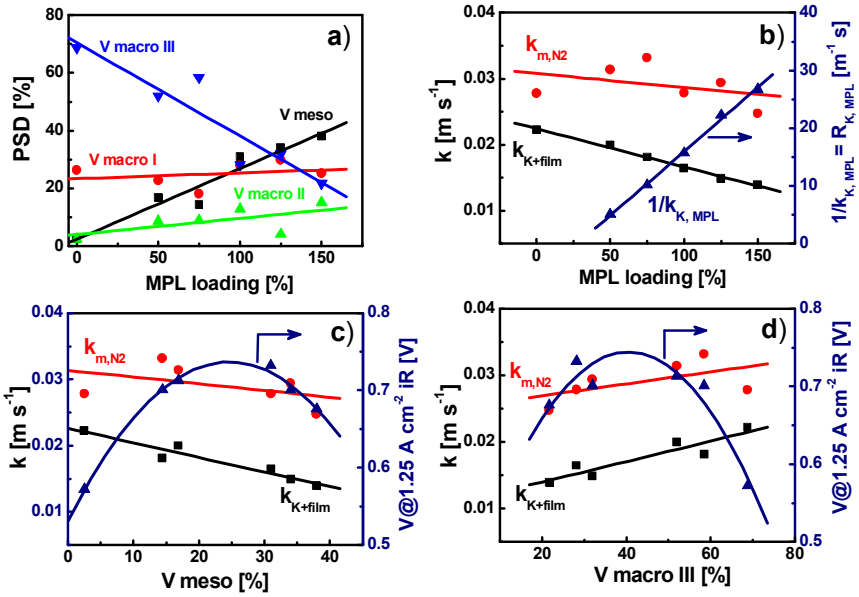

Fig. 4. Structure-to-properties correlations. Anode/cathode: H_2/air, 2/2 stoichiometry, 100/100% RH, 150/150 kPa, 60°C.

3.3.3. Subtask 1.3. Limiting current density distribution and EIS

To accomplish this subtask the work was divided into two directions. First, the proposed method of calculating of oxygen mass transfer coefficient was applied to characterize performance of Nuvera's single cell open flow field (SCOF) hardware. The developed SCOF is known for ensuring excellent PEMFC performance at high-power operating conditions at current densities ≥ 3 A cm^{-2}. Thus, SCOF possesses outstanding gas and water management properties and is the best choice for validation of our method. Second, a previous publication on evaluation of SCOF showed possibility of application of EIS and subsequent impedance spectra modeling for extracting mass transfer parameters [12]. This paper inspired us to start developing impedance models based on a physical representation of the processes occurring in the membrane electrode assembly (MEA) for validation of the results obtained by the proposed limiting current distribution method.

For this work commercial Gore MEA with active area of 50 cm^2 and with anode and cathode Pt loadings of 0.1 and 0.4 mg Pt cm^{-2}, respectively, was used. Membrane was mechanically and chemically reinforced with thickness of 18 μm. Freudenberg H1410I4 C10 GDLs (microporous layer + hydrophobic treatment) with 150 μm thick was applied for both electrodes. Results of the initial diagnostics relevant for SCOF and performed at HiSERF were close to the results provided by Nuvera. SCOF did not have a segmented flow field, so oxygen mass transfer coefficient was calculated using the average limiting current density i_{ave} model (Eqs. 2, 3). This approach provided us O_2 mass transport coefficient values: k_{K+film} was found to be 0.01336 m s^{-1}, while $k_{m,\,N2}$ was 0.02805 m s^{-1} at best performing operating parameters (80°C, 50% RH, high back pressure). At 60°C and fully humidified conditions, k_{K+film} equals to 0.00694 m s^{-1}, molecular mass transport in N_2 media is 0.0335 m s^{-1}. Interestingly, that best performing operating conditions determined by Nuvera ensured high values of the mass transport coefficients compared to the case of 60°C.

For analysis of EIS data of Nuvera's SCOF a previously described model was applied [13]. The impedance model is based on the standard transient macrohomogeneous model for the cathode catalyst layer (CCL) performance [14-16] and includes oxygen and proton transport equations in the cathode layer, Volmer equation for the rate of the ORR:

$$C_{dl}\frac{\partial \eta}{\partial t}+\frac{\partial j}{\partial x}=-2i_*\left(\frac{c}{c_h^{in}}\right)sinh\left(\frac{\eta}{b}\right) \quad (9)$$

$$j=-\sigma_p(x)\frac{\partial \eta}{\partial x} \quad (10)$$

$$\frac{\partial c}{\partial t}-D_{ox}\frac{\partial^2 c}{\partial x^2}=-\frac{2i_*}{4F}\left(\frac{c}{c_h^{in}}\right)\sinh\left(\frac{\eta}{b}\right) \quad (11)$$

Here C_{dl} is the double layer volumetric capacitance (F cm^{-3}),
η is the ORR overpotential, positive by convention,
t is time,
j is the local proton current density,
x is the distance through the MEA from the membrane interface,
i_* is the volumetric exchange current density (A cm^{-3}),
c is the local oxygen concentration,
$c^{in}{}_h$ is its reference (inlet) concentration,
b is the Tafel slope,
σ_p is the CCL proton conductivity,
D_{ox} is the effective oxygen diffusion coefficient in the CCL.

We assume that proton conductivity is an exponential function of coordinate x [17]:

$$\sigma_p=\sigma_{p,0}exp\left(-7.3\frac{x}{l_t}\right) \quad (12)$$

where l_t is the CCL thickness.

The equation for oxygen transport in the GDL is described by Fick's law:

$$\frac{\partial c_b}{\partial t}-D_b\frac{\partial^2 c_b}{\partial x^2}=0 \quad (13)$$

where c_b is the oxygen concentration in the GDL,

D_b is the oxygen diffusion coefficient in the GDL.

The system of Eqs. 9-13 has been linearized and Fourier-transformed. The resulting system of linear equations for the perturbation amplitudes has been solved numerically. Fitting experimental impedance spectra provided kinetic (Tafel slope) and transport parameters (double layer capacitance, proton conductivity, oxygen transport through CCL and GDL).

Based on EIS data the oxygen mass transfer coefficient in CCL varies in the range of 0.0002-0.004 m s^{-1} depending on operating current. These mass transfer coefficients are lower than k_{K+film} obtained by limiting current approach (0.01336 m s^{-1} (80°C) and 0.00695 m s^{-1} (60°C)). The discrepancy in the data can be attributed to the experimental conditions of EIS and limiting current experiments. In the case of EIS the cell was running using air, while for the limiting current method diluted mixtures (5% O_2) were applied to cathode. It is clear that at regular conditions excess of water production and liquid water formation is highly possible which impedes diffusion processes and results in lower oxygen mass transfer coefficient values. While at the conditions of limiting current operation, it is likely that liquid water accumulation is low since total cell current density is in the range of 0.27-0.45 A cm^{-2}.

A comparison of results on O_2 mass transfer obtained by EIS and limiting current approaches showed that we are performing experiments at different conditions and it is impossible to directly compare the data. After discussion and deep consideration, we concluded that the limiting current method as well as EIS modeling provide reliable representative results for conditions applicable for techniques and the methods do not contradict but complement each other. So, we continued developing EIS models, since EIS is non-invasive and non-destructive technique which allows measuring key electrochemical parameters in a working cell in operando conditions. Thus, developing of physics-based EIS models can provide realistic on-line information about working electrode. The details of this work can be found in our publications [13, 17-21].

3.4. Task 2. Method development

3.4.1. Subtask 2.1. Simplification of the mass transfer coefficient separation method

Simplification of the local limiting current distribution separation method was achieved by eliminating most of the expensive gas diluents like Ne ($4,194), Kr ($10,498), SF_6 ($3,275) and possibly C_3F_8 ($4,567). Data for three MEAs was analyzed by decreasing the number of gas diluents from 9 to 4 and 3 (respectively He-N_2-Ar-C_3F_8 and He-N_2-C_3F_8 with He-C_3F_8 denoting the 9 diluents case). Results indicated that the decrease to 3 or 4 diluents provide the close values of mass transfer coefficients for the studied MEAs. For the practical use, a decrease in the number of gas diluents to 3 (He-N_2-C_3F_8) would reduce cost and testing time while minimally impacting measurement accuracy.

3.4.2. Subtask 2.2. Extension of the applicability range of the method

The dilute reactant stream model (Eq. 1) was expanded to the mixed control by substituting the following equation containing Tafel (i_K) and mass transfer contributions (i_{lim}):

$$i = \frac{1}{(1/i_{lim} + 1/i_k)} \quad (14)$$

Reference [22] provides details of the mathematical transformations and the derivation that yields the final current distribution:

$$\tilde{x} = i_e \left[\left(\frac{1}{i_k} - \frac{1}{i_{lim,0}} \left(\frac{i}{i_k - i} \right) \right) + \frac{1}{i_{lim,0}} \ln \left(\frac{i_{lim,0}}{i} - \frac{i_{lim,0}}{i_k} \right) \right] \quad (15)$$

Eq. 15 contains 2 unknown parameters (i_k, $i_{lim,0}$) which are obtained by curve fitting. The overall oxygen mass transfer coefficient was obtained from $i_{lim,0}$ values using Eq. 16 and cell operating conditions.

$$i_{lim,0} = \frac{nFkp_r}{RTf} \quad (16)$$

The extended model was validated using experimental data and results were discussed in [22].

3.4.3. Subtask 2.3. Impact of operating conditions on mass transport mechanisms

To evaluate the effects of relative humidity and back pressure we used Gore MEAs with anode and cathode loadings of 0.1 and 0.2 mg_{Pt} cm^{-2} and thicknesses of 3-4 and 6-7 µm, respectively. Cathode GDLs were also varied to elucidate impacts of MPL and CL. So, we used 25BA and 25BC diffusion medias with thicknesses of 180 and 235 µm. Thus, operation of MEA-25BA provided us with results on mass transport predominantly in the catalyst layer, since GDL does not include MPL. The experiments were performed at two operating temperatures: 60 and 80°C.

3.4.3.1. Impacts of gas humidification

In our testing matrix we used three values of reagent humidification: 32, 50 and 100% RH for fuel and oxidant streams. Reagents humidification affects the cell performance in several ways [23]. Due to insufficient humidification of electrodes ECA appears to be low and causes an increase in activation losses. Moreover, low RH increases high frequency resistance (HFR) and accordingly to leads to greater ohmic overpotential. Impact of reagent humidification on mass transport is complex. On one hand, excessive water leads to cell flooding and increases mass transport overpotential. However, humidification also seriously modifies Nafion gas permeability: a reduction of water content in a gas stream negatively affects gas transport through the ionomer and causes PEMFC performance decline also due to increasing mass transport losses [24]. So, the impact of RH on oxygen mass transport in GDE appears to be of particular interest for an understanding the fundamentals of the gas transport in confined multiphase porous structure.

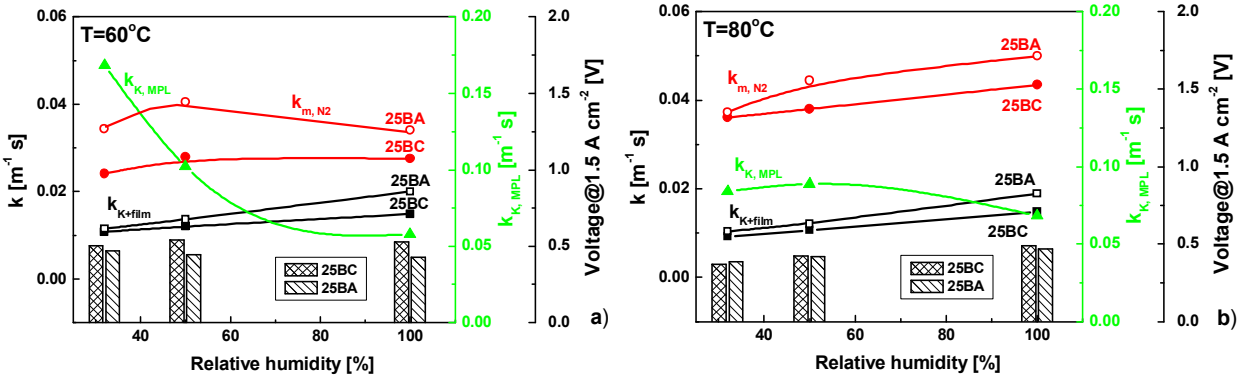

Fig. 5. Effects of humidification on the oxygen mass transfer coefficients and performance at 60 (a) and 80°C (b).

The oxygen mass transfer coefficient in the gas phase (N_2) was found to grow when RH increased from 32 to 50% at 60°C, but further increases in gas humidification did not affect its value (Fig. 5 a). At the same time, operation at 80°C demonstrated an increase in $k_{m,\,N2}$ with humidification (Fig. 5 b). Behavior of $k_{K,\,MPL}$ showed a similar development at both temperatures: a decrease in oxygen transport with RH. In addition, an increase in RH also positively impacted k_{K+film}. The observed trends in mass transfer coefficients with RH and temperature can be attributed to gas permeability of the Nafion and its dependence on humidification, which is more critical at low RH operation. Higher RH effects are associated with liquid water formation and its removal through the evaporation mechanism as well as though liquid-phase motion due to capillary effects of MPL [25, 26]. Apparently, water effects seem to be more pronounced at 60°C, where mass transfer coefficients in the gas phase and in MPL are decreasing with RH. Higher operating temperature appears to be beneficial for oxygen transport in GDE and results in greater values of the mass transfer coefficients in the gas phase ($k_{m,\,N2}$).

3.4.3.2. Impacts of back pressure

To understand effects of back pressure on PEMFC performance and oxygen transport the following values of gauged back pressure (BP) were used: 0, 50, 100 and 150 kPa_g simultaneously for anode and cathode. Variation in back pressure leads to separation the total transport resistance into pressure-dependent and pressure-independent components and further analyze the oxygen transport. It was found that the overall oxygen resistance is proportional to total back pressure for various diluents (He, N_2, Ar, CF_4, SF_6 and C_3F_8) [10, 11, 28]. This observation is a good indication that water does not condense in the cell and the transport properties are the same at all operating conditions. We assume that the total transport resistance may be decomposed into pressure-dependent and pressure-independent components according to:

$$\frac{1}{k} = \frac{1}{k^{pr-ind}} + \frac{1}{k^{pr}} P \qquad (17)$$

Pressure-independent contributions to the oxygen mass transport can be attained from extrapolated intercepts. Interestingly, the intercept values were found to be positive for He, N_2 and Ar diluents, while for CF_4, SF_6 and C_3F_8 its values were negative. The observation implies that for these heavy diluents O_2 diffusion in GDE is completely controlled by molecular diffusion.

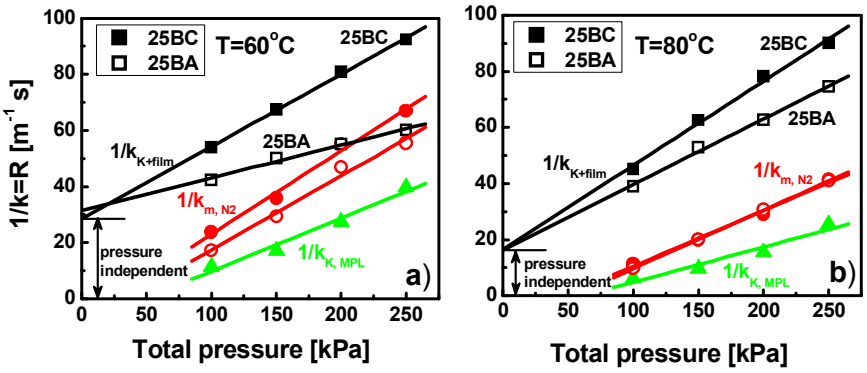

Fig. 6. Oxygen mass transport coefficient (a, b) as functions of back pressure and temperature.

To understand effects of back pressure on mass transport processes we analyzed dependence of R_{K+film}, $R_{m,\ N2}$, $R_{K,\ MPL}$ vs total pressure (Fig. 6). Linear regressions for $Rk_{K,\ MPL}$ and $Rk_{m,\ N2}$ have negative intercepts which does not have physical meaning and implies that these parameters are completely pressure-dependent. Only a linear interpolation for Rk_{K+film} returns with positive intercepts. These findings suggest that k_{K+film} value obtained by our method (limiting current distribution with varied dilents) includes some pressure-dependent and pressure-independent components. On the first glance the observation that k_{K+film} and $k_{K,\ MPL}$ are pressure-dependent was surprising, since Knudsen diffusion does not depend on pressure:

$$D_K = \frac{l}{3}\sqrt{\frac{8RT}{\pi M}} \tag{18}$$

where l is the pore diameter and M is the molecular weight of species.

However, by definition, Knudsen diffusion occurs when the molecular mean free path is much larger than the diameter of the pore in which the diffusing molecules reside, the molecules collide with the wall rather than colliding with other molecules. However, strictly speaking mean free path (λ) is a function of pressure:

$$\lambda = \frac{kT}{\sqrt{2}\pi d^2 p} \tag{19}$$

where k is Boltzmann constant, T is a temperature, d is an effective cross-sectional diameter for particles, p is a pressure. So, Knudsen number, which is a ratio of the mean free path and pore diameter, is also a pressure-dependent function.

$$K_n = \frac{\lambda}{l} \propto \frac{1}{p} \tag{20}$$

This means that the distance of Knudsen diffusion should vary with overall pressure and explains the obtained dependences at Fig. 6. Nevertheless, the pressure-independent contributions, $k_{K+film}^{pr\text{-}ind}$, for MEA-25BA and MEA-25BC seem to be very close and are most likely related to O_2 transport through ionomer-water film (Fig. 6 a and b). This pressure-independent oxygen mass transport coefficient increases with operating temperature and equals to 0.032 and 0.061 m s^{-1} for 60 and 80°C, respectively. Thus, variation of back pressure allowed us to determine and extract the pressure-independent component of oxygen transport and further separate Knudsen diffusion from diffusion through ionomer-water films.

3.4.4. Subtask 2.4. Effects of ionomer loading and electrode structure

In the frame of this subtask we compared oxygen mass transfer properties of Gore electrodes and 3M nano-structured thin film (NSTF) [29]. For the conventional Gore catalyst coated membrane (CCM) cathode Pt loading was 0.1, 0.2 and 0.4 mg cm^{-2}, while the anode Pt content was kept 0.1 mg cm^{-2}. MEA from 3M had Pt-Co-Mn based catalyst with loadings of 0.15 mg cm^{-2} for cathode and 0.05 mg cm^{-2} for anode. NSTF MEAs were assembled with 3M designed GDLs which we denoted as 3M-GDLs. In addition, we studied 3M and Gore MEAs with 25BA as a cathode GDL to extract oxygen transport parameters in electrode structures. Using the above-described methodology (variation of O_2 diluents and cell back pressure) we determined oxygen mass transport coefficients for samples with 25BA and 25BC (or 3M-GDL) gas diffusion media.

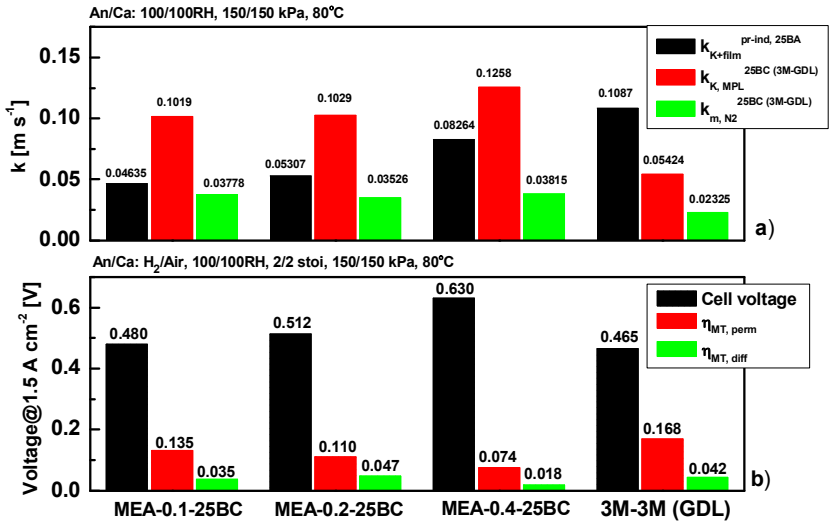

Fig. 7. A comparison of oxygen mass transfer coefficients (a), performance and voltage losses (b) for samples with different Pt cathode loadings.

The obtained values of pressure-independent oxygen mass transfer coefficients in catalyst layer ($k_{K+film}^{pr\text{-}ind,\ 25BA}$), O_2 diffusion in MPL ($k_{K,\ MPL}^{25BC}$) and molecular diffusion in N_2 media ($k_{m,\ N2}^{25BC}$) at 150 kPa and 100%RH are compared at Fig. 7 a. A decrease in Pt loading for conventional Gore MEAs results in a decrease in $k_{K+film}^{pr\text{-}ind,25BA}$ as it was previously reported [7, 30-32]. Interestingly, 3M-3M-GDL sample has the greatest value of $k_{K+film}^{pr\text{-}ind,\ 25BA}$ of 0.1087 m s^{-1}. Gore MEAs are characterized by quite close $k_{m,\ N2}^{25BC}$, while 3M sample shows the lowest values of O_2 transport in the gas phase. Performances of the studied samples in terms of cell voltage at 1.5 A cm^{-2} and voltage losses (mass-transport: permeability and diffusion) are presented at Fig. 7 b. A direct comparison of the performances and oxygen mass transfer coefficients shows MEA-0.4-25BC had the best performance, whereas the worst performance was observed for 3M-3M-GDL at the chosen operation conditions. Among Gore MEAs the highest performance of MEA-0.4-25BC could be attributed to the greatest value of $k_{K+film}^{pr\text{-}ind,\ 25BA}$ insuring a good gas transport within catalyst layer as well as water transport. In spite of the highest $k_{K+film}^{pr\text{-}ind,\ 25BA}$ value, 3M-3M performance was the lowest among the all samples. In addition, 3M-3M-GDL sample has the lowest values of $k_{K,\ MPL}^{3M\text{-}GDL}$ and $k_{m,\ N2}^{3M\text{-}GDL}$ and the highest values of voltage losses. Hence, it is possible to speculate that for 3M gas diffusion is hindered most likely due to excess of water at the fully humidified conditions.

In order to study effects of humidification on 3M NSTF MEAs we used 32, 50 and 100% RH for fuel and oxidant streams. In conventional electrodes, like Gore, the ionomer binder percolates within meso- and macroporous electrode's textural matrix and the ionomer insures high proton concentration and good proton transport. In NSTF electrodes there is no ionomer to assist in proton conduction which seriously affects the NSTF performance at low humidification [29, 33]. The impact of RH on oxygen mass transport in 3M electrodes appears to be of particular interest for understanding the gas and proton transport in such porous structures.

Fig. 8 presents a comparison of the mass transport coefficients at different RHs and the performance of 3M-3M-GDL sample at high current density of 1.5 A cm^{-2} together with performance deconvolution in terms of voltage losses. As it was mentioned earlier, the low reagents humidification caused low ECA and an increase in activation losses. Moreover, low RH led to higher HFR and ohmic

overpotential. In addition, a decrease in initial gas humidification resulted in a growth of cumulative mass transfer losses ($\eta_{MT,\ perm} + \eta_{MT,\ diff}$) for NSTF MEAs [33] (Fig. 8 b). A comparison of the performance and oxygen mass transfer coefficients clearly showed that low RH led to a decrease in $k_{K+film}^{pr\text{-}ind,\ 25BA}$ and an increase in mass transfer overpotentials which could be explained by to poor oxygen diffusivity for membrane embedded whisker area and poor proton conductivity for the whisker outside the membrane area. Oxygen transport in the gas phase $k_{m,\ N2}^{3M\text{-}GDL}$ decreases slightly with humidification due to excess of water in gas stream.

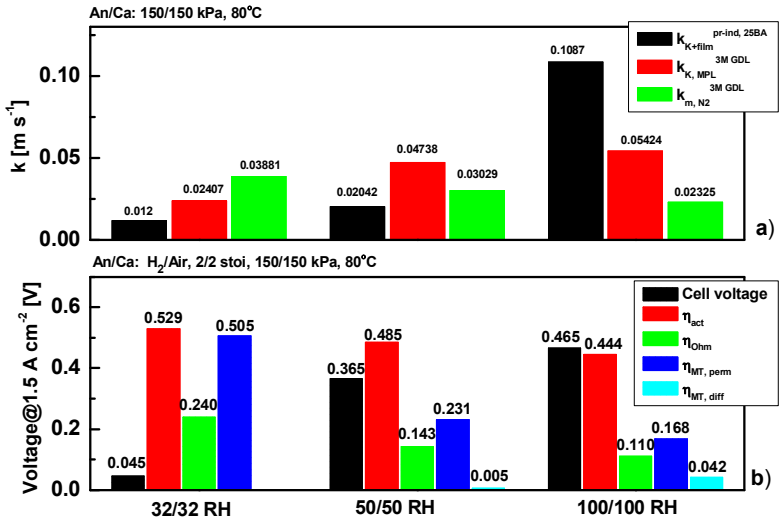

Fig. 8. A comparison of oxygen mass transfer coefficients (a), performance and voltage losses (b) for NSTF MEAs at different RH.

3.4.5. Subtask 2.5. Application of the method to determine H_2 mass transport processes

To validate the proposed method for determining H_2 mass transport parameters we used Gore MEA with anode and cathode loadings of 0.4 mg_{Pt} cm^{-2}. We applied 25BC and 25BA GDLs for anode to separate effect of MPL on hydrogen mass transport. The samples are denoted as MEA-0.4-25BC and MEA-0.4-25BA. Limiting current measurements were done in passive or H_2 pump mode and with fully humidified reagents (100% RH). H_2 crossover current was determined by linear sweep voltammetry for each operating condition to correct the spatial limiting currents. Typically, H_2 crossover current depends on temperature, humidification and back pressure and at the chosen operating conditions it varied from 1.3 mA cm^{-2} (35°C, ambient pressure) to 8.2 mA cm^{-2} (80°C, 150 kPa_g). Fig. 9 presents typical spatial IV curves recorded at limiting current conditions and results of the fitting.

It was also found a clear linear correlation between H_2 mass transfer resistance and diluent molecular weight which allowed us to separate H_2 molecular diffusion from Knudsen and film diffusion similar to O_2 case (Fig. 10 a). Moreover, dependence of H_2 mass transport resistance vs back pressure revealed a linear relationship (Fig. 10 b). These findings were also observed for sample MEA-0.4-25BA and allowed us to deconvole hydrogen mass transport resistance in the gas phase (k_m), MPL (k_{MPL}^{25BC}), through ionomer/water films in the electrode ($k_{K+film}^{pr\text{-}ind}$). Table 3 summarize the obtained

data for mass transfer coefficients. The H_2 mass transport coefficients are in a good agreement with results published in the literature [34-36].

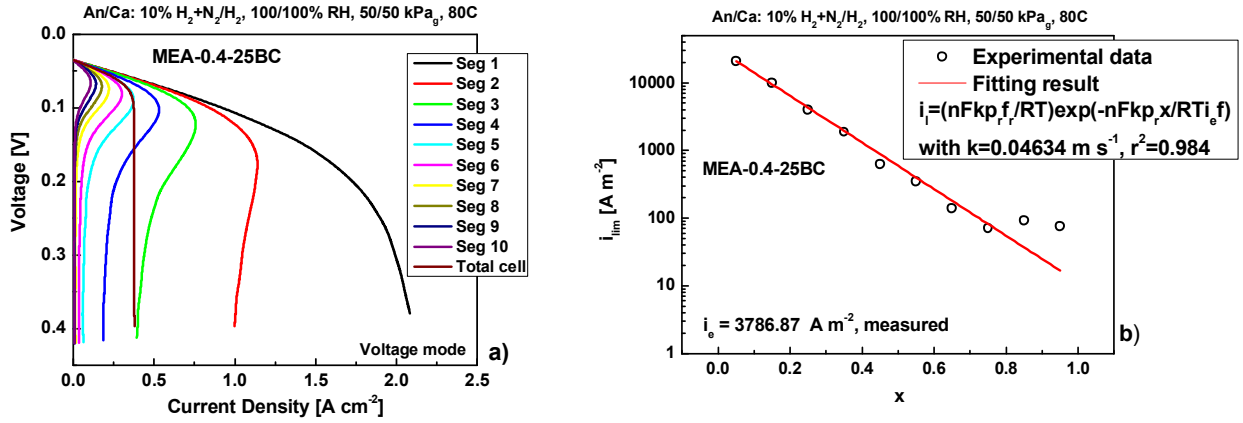

Fig. 9. IV curves for individual segments (a) and fitting of the experimental data to the model (b). An/Ca: 10%H_2 + N_2/H_2, 0.2 +1.8/0.5 slpm, 100/100RH, 150/150 kPa, 80°C.

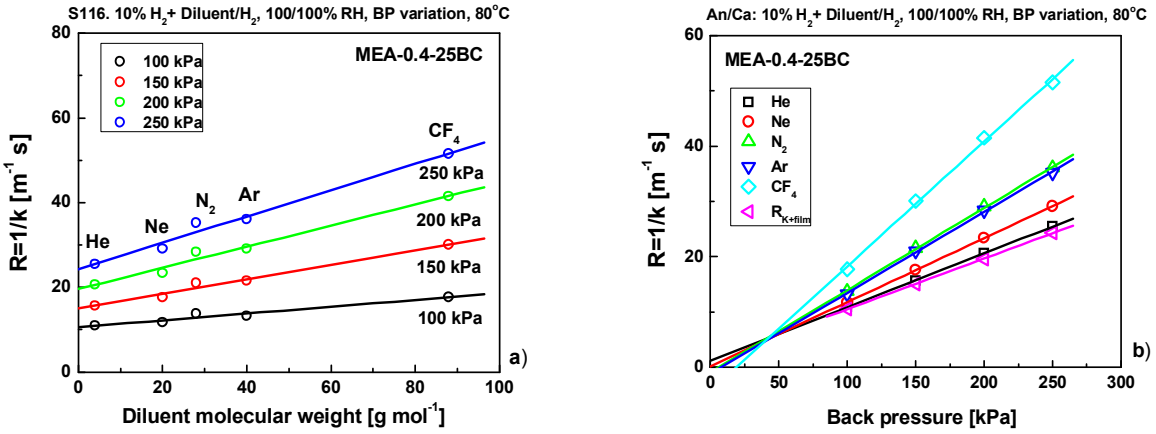

Fig. 10. Hydrogen mass transport resistance as function of diluent molecular weight (a) and dependence of the mass transport resistance from back pressure for various diluents (b). An/Ca: 10%H_2 + Diluent/H_2, 0.2 +1.8/0.5 slpm, 100/100RH, 80°C.

Table 3. H_2 and D_2 mass transfer coefficients in He and N_2 media (k_m), cumulative value for Knudsen and film diffusion (k_{K+film}), through ionomer/water films in the electrode ($k_{K+film}^{pr\text{-}ind}$) and contribution originating from MPL ($k_{K,\,MPL}$). Anode/cathode: 10%H_2 (or D_2) + Diluent/H_2, 100/100% RH, 80°C.

Sample	BP [kPa_g]	k_{K+film} [$m\ s^{-1}$]	$k_{m,\,N2}$ [$m\ s^{-1}$]	$k_{m,\,He}$ [$m\ s^{-1}$]	$k_{K,\,MPL}$ [$m\ s^{-1}$]	$k_{K+film}^{pr\text{-}ind}$ [$m\ s^{-1}$]
Hydrogen						
MEA-0.4-25BC	0	0.09425	0.8776	2.7893	0.7028	0.7084
	50	0.0664	0.3863	1.6839	0.8253	
	100	0.05096	0.2641	0.9909	0.5470	
	150	0.04112	0.2075	0.8617	0.4082	
MEA-0.4-25BA	0	0.10885	1.1465	3.1038		1.0219
	50	0.07221	0.4239	2.9098		
	100	0.05619	0.2728	1.2232		
	150	0.04573	0.2217	0.7037		
Deuterium						
MEA-0.4-25BC	0	0.07101	0.5132	1.4894	0.4231	0.5875
	50	0.05058	0.2375	1.6637	0.3714	
	100	0.03883	0.1945	1.2685	0.2655	
	150	0.0309	0.1398	0.7859	0.2179	
MEA-0.4-25BA	0	0.08533	0.6256	2.8478		0.9408
	50	0.05856	0.2760	2.2455		
	100	0.04548	0.1793	1.7017		
	150	0.036	0.1447	0.7474		

Switching the reactant gas from H_2 to D_2 or O_2 can determine to which extent the transport resistances depend on reagent molecular weight. Fig. 11 illustrates a comparison of the mass transport coefficients calculated for these three gases as functions of back pressure. It is clear that mass transport resistance increased with molecular weight. For example, the molecular resistance in N_2 ($k_{m,\,N2}$) increased by a factor of around $\sqrt{2}$ when replacing H_2 by D_2 due to the fact that the molecular diffusion is controlled by diffusion coefficient. The molecular diffusion coefficient can be estimated using the Chapman-Enskog theory [37]:

$$D_{A,B} = \frac{0.0018583}{p\sigma_{AB}\Omega_{D,AB}}\sqrt{T^3\left(\frac{1}{M_A}+\frac{1}{M_B}\right)} \qquad (22)$$

where T is temperature of the gas in units of Kelvin, M_A and M_B are molecular weights of species A and B, p is the total pressure of the binary mixture in units of atmospheres, σ_{AB} is the Lennard-Jones force constant for the gas mixture and $\Omega_{D,\,AB}$ is the collision integral.

So, changing the reacting gas from H_2 to D_2 or O_2 whose molecular weight is twice (D_2) or 16-times (O_2) higher should lower the diffusion coefficient by factor $\sqrt{2}$ or $\sqrt{16}$, respectively. However, in the case of O_2 one could observe quite significant growth in mass transport resistance (by factor of ~10). The possible explanation for this discrepancy could be due to processes on Pt surface like adsorption/desorption which occur differently for HOR and ORR. Also, we need to consider that the gas phase is not a perfect mixture of two components, there is a water vapor which brings additional complexity.

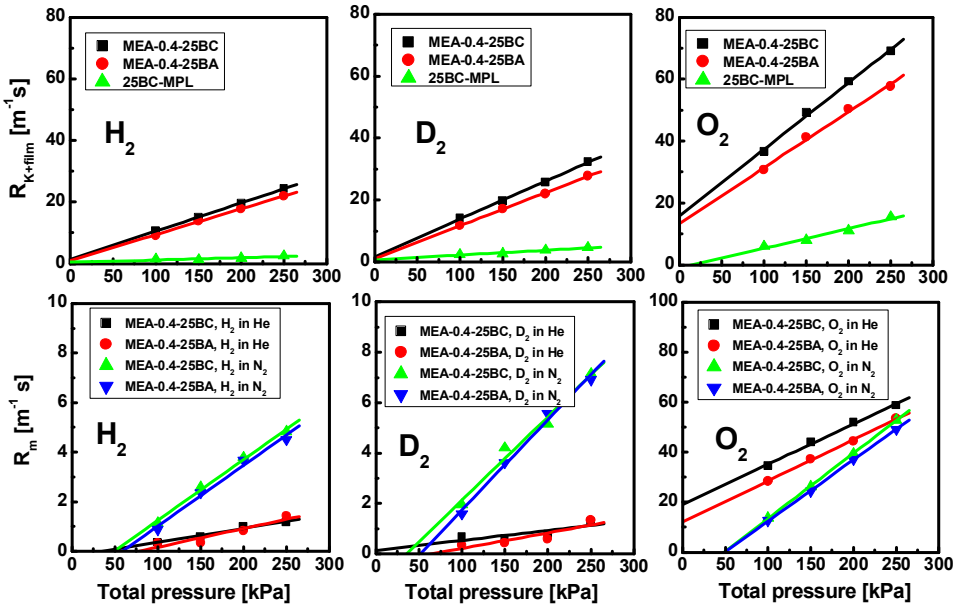

Fig. 11. Dependence of mass transfer resistances from back pressure for different reacting gas: H_2, D_2 and O_2.

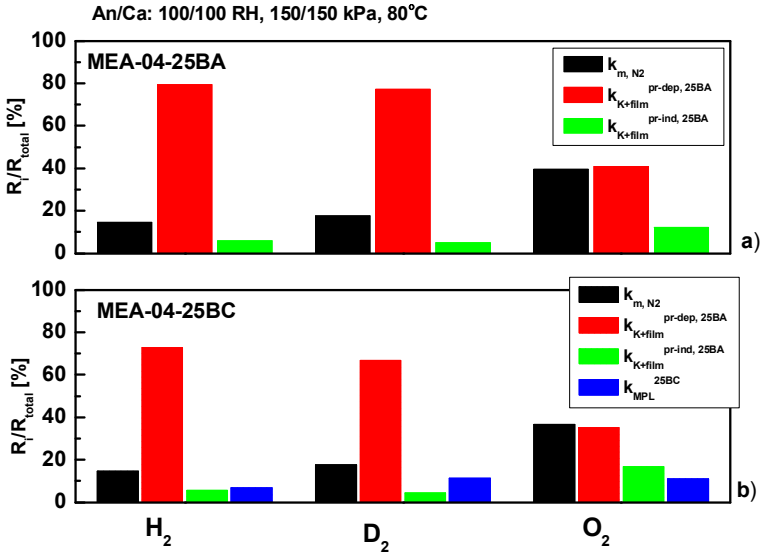

Fig. 12. Breakdown of GDE resistance into contributing components.

Breakdown of GDE resistance arising from the gas phase ($k_{m,\,N2}$), MPL (k_{MPL}^{25BC}), transport through films in the electrode ($k_{K+film}^{pr\text{-}ind,\,25BA}$) and Knudsen diffusion in CL ($k_{K+film}^{pr\text{-}dep,\,25BA}$) are presented at Fig. 12. Interestingly, for the light reactant molecules (H_2 and D_2) the main contribution to transport resistance comes from pressure-dependent diffusion in electrode, while for O_2 contributions from molecular diffusion accounts for 36%.

The results of this subtask are clearly showing that the proposed methodology is applicable for determining H_2 mass transport characteristics. Moreover, to the best of our knowledge, this is the only

approach which allows us to directly measure H_2 mass transport properties in real working MEA as a part of routine diagnostics, while the currently described method requires sophisticated and complex hardware and allowing measurements at low temperature range [34, 35]. Thus, the method can be easily adopted and applied for fuel or oxidant reactant gas and all tests can be done with one MEA sample.

3.5. Task 3. Outreach

3.5.1. Technology transition

Recipients: Nuvera Inc, 3M

The methodology was successfully applied to Nuvera's single cell open flow field (SCOF) design and 3M nanostructured thin film (NSTF) membrane/electrode assemblies (MEAs) to study mass transport phenomena. These results transitioned to Nuvera and 3M for further validation and use of the methodology to understand mass transport issues in PEMFCs.

3.5.2. Awards and recognitions

1. Keynote presentation at International workshop on Energy, Environment, Water and Sustainability (EEWS) - 2015 at Korean Advanced Institute of Science and Technology (KAIST), December 4, 2015, Daejeon, South Korea.
2. Invited presentation at Gordon Research Conference-2016 (Fuel cell), August 7-12, 2016, Easton, MA.

3.5.3. Publications

1. T. Reshetenko, A. Kulikovsky, *"Comparison of two physical models for fitting PEM fuel cell impedance spectra measured at low air flow stoichiometry"*, J. Electrochem. Soc. 163 (2016) F238.
2. T. Reshetenko, A. Kulikovsky, *"Variation of PEM fuel cell physical parameters with current: Impedance spectroscopy study",* J. Electrochem. Soc. 163 (2016) F1100.
3. J. St-Pierre, T.V. Reshetenko, *"PEMFC reactant mass transfer coefficient measurement and separation – method extension to the mixed kinetic and mass transfer control regime"*, ECS Trans. 75 (14) (2016) 63.
4. T. Reshetenko, A. Kulikovsky, *"Impedance spectroscopy characterization of oxygen transport in low- and high-Pt loaded PEM fuel cells"*, J. Electrochem. Soc. 164 (2017) F1633.
5. T. Reshetenko, A. Kulikovsky, *"Impedance spectroscopy study of the PEM fuel cell cathode with nonuniform nafion loading"*, J. Electrochem. Soc. 164 (2017) E3016.
6. T. Reshetenko, A. Kulikovsky, *"Two states of the cathode catalyst layer operation in a PEM fuel cell"*, J. Electrochem. Soc. 165 (2018) F821.
7. T. Reshetenko, A. Kulikovsky, *"A model for extraction of spatially resolved data from impedance spectrum of a PEM fuel cell"*, J. Electrochem. Soc. 165 (2018) F291.
8. T. Reshetenko, A. Kulikovsky, *"On the distribution of local current density along a PEM fuel cell cathode channel"*, Electrochem. Commun. 101 (2019) 35.
9. T. Reshetenko, A. Kulikovsky, *"A model for local impedance: Validation of the model for local parameters recovery from a single spectrum of PEM fuel cell"*, J. Electrochem. Soc. 166 (2019) F431.

10. T. Reshetenko, A. Kulikovsky, *"On the origin of high frequency impedance feature in a PEM fuel cell"*, J. Electrochemical Soc. 166 (2019) F1253.
11. T. Reshetenko, A. Kulikovsky, *"Nafion film transport properties in a low-Pt PEM fuel cell: Impedance spectroscopy study"*, RSC Advances 9 (2019) 38797.

3.5.4. Presentations

1. T.V. Reshetenko, K. Bethune, G. Randolf, J. St-Pierre, *"Understanding spatial PEMFCs performance under different environmental and operating conditions using a segmented cell approach"*, International workshop on EEWS-2015 at KAIST, December 4, 2015, Daejeon, South Korea, Keynote speaker.
2. T.V. Reshetenko, J. St-Pierre, A. Kulikovsky, *"Determination and separation of PEMFC reagents mass transport coefficients by localized limiting current approach"*, Gordon Research Conference-2016 (Fuel cell), August 7-12, 2016, Easton, MA, Invited speaker.
3. J. St-Pierre, T.V. Reshetenko, *"PEMFC reactant mass transfer coefficient measurement and separation – method extension to the mixed kinetic and mass transfer control regime"*, 230th ECS Meeting, October 2-7, 2016, Honolulu, HI, I01-2356.
4. J. St-Pierre, T. Reshetenko, "*O_2 mass transfer coefficient in PEMFCs – cell voltage and MEA effects"*, ECS-CSE Joint Symposium on Electrochemistry of Energy & Environment, Shanghai, China, December 2-4, 2017, Paper # EC-16.
5. T.V. Reshetenko, B.L. Ben, *"Effects of structural and textural properties of GDL on oxygen mass transport coefficient in PEMFC"*, Gordon Research Conference-2018 (Fuel cell), Jul. 29 – Aug. 3, 2018. Smithfield, RI.
6. T.V. Reshetenko, B.L. Ben, "*Analysis of mass transport phenomena in PEMFC cathode electrode: Effects of operating conditions*" 236th ECS Meeting, October 13-17, 2019, Atlanta, GA, I01A-1449.

3.5.5. Publications in preparation

1. T.V. Reshetenko, B.L. Ben, *"Impacts of structural and textural properties of GDL on oxygen mass transport processes in PEMFC"*, in preparation.
2. T.V. Reshetenko, B.L. Ben, *"Effects of operating conditions on mass transport phenomena in PEMFC cathode electrode*", in preparation.
3. T.V. Reshetenko, B.L. Ben, *"PEMFC gas diffusion electrode structure and oxygen mass transport*", in preparation.
4. T.V. Reshetenko, *"Application of hydrogen and oxygen limiting current distributions for elucidating mass transport in PEMFCs"*, in preparation.
5. T.V. Reshetenko, O. Polevaya, A. Kulikovsky, *"Model-based impedance of the cathode proton conductivity in operating PEM fuel cell"*, in preparation.

4. Summary and Conclusions

1. Method validation

1.1. The validity of the method was demonstrated and proven using commercially relevant flow field design developed by Nuvera Fuel Cell and membrane/electrode assemblies with different electrode structures provided by Gore and 3M. Reproducibility of oxygen mass transfer coefficient determination methods was successfully demonstrated using 1) local limiting current distribution and 2) average limiting current mathematical models.

1.2. Effects of MPL in GDL on the oxygen mass transfer coefficient were studied. An increase in MPL loadings in an electrode structure decreased the gas phase molecular diffusion as well as Knudsen and film diffusion and affected performance. There is an optimal MPL content which provides desirable mass transfer properties and high performance. Moreover, the results provided an approach on further quantitative separation of different electrode components contribution to mass transfer.

1.3. Impedance models based on a physical representation of the processes in the MEAs were developed for validation of the results obtained by the proposed limiting current distribution method. The impedance modeling approach allows kinetic and transport parameters (oxygen diffusion as well as proton conductivity) to be determined on-line in operando conditions. The EIS modeling results complemented limiting current methodology.

2. Method development

2.1. Separation of the overall O_2 mass transfer coefficient into the gas phase and a combination of Knudsen and film diffusion was simplified by decreasing the number of gas diluents from 9 to 3 (He, N_2 and C_3F_8) without losing quality.

2.2. The applicability range of the model to the mixed kinetic and mass transfer control dependent local current was expanded by including Tafel and mass transfer contributions. The extended model was validated using experimental data.

2.3. Impacts of fuel cell operating conditions such as cell temperature, gas humidification and total back pressure on the oxygen mass transfer coefficients were studied in details. An increase in reagent humidification resulted in better oxygen transport in the gas phase as well as in confined pores and through films. Variation of back pressure allowed us to determine the pressure-independent component of oxygen transport and further separate Knudsen diffusion from diffusion through ionomer/water films. The developed structure-to-properties correlations provide interplay between operating conditions, oxygen transport and fuel cell performance.

2.4. Effects of ionomer in the electrode structure on the oxygen mass transfer coefficients were evaluated using NSTF MEAs from 3M and regular ionomer ink catalyst layers (Gore MEAs). A comparison of the different electrode structures showed that NSTF were characterized by the greatest k_{K+film} value of 0.1087 vs 0.05307 m s^{-1} for Gore catalyst layer with close Pt loading. At the same time, NSTF electrodes demonstrated variation in $k_{m,\ N2}$ and lower value of $k_{K,\ MPL}$ compared to Gore samples, which explained the observed differences in performance.

2.5. The proposed method was successfully applied to gain knowledge on H_2 mass transport processes. Optimal operating conditions were established and recommendations on the procedure were developed. The work pioneered in development and application distribution of limiting current for analyzing H_2 mass transport in realistic operating condition of working electrode structures.

3. There were 11 published papers in J. Electrochem. Soc, ESC Trans., Electrochem. Commun., RCS Advances and 6 delivered presentations.

5. Supported personnel

Tatyana Reshetenko, 33% supported, 33% Full Time Equivalent (FTE) support provided by this agreement in 2015.
Tatyana Reshetenko, 47% supported, 47% Full Time Equivalent (FTE) support provided by this agreement in 2016.
Tatyana Reshetenko, 46% supported, 46% Full Time Equivalent (FTE) support provided by this agreement in 2017.
Tatyana Reshetenko, 23% supported, 23% Full Time Equivalent (FTE) support provided by this agreement in 2018.

6. Bibliography

[1] L. Cindrella, A.M. Kannan, J.F. Lin, K. Saminathan, Y. Ho, C.W. Lin, J. Wertz, J. Power Sources 194 (2009) 146.
[2] M.F. Mathias, J. Roth, J. Fleming, W. Lehnert, in "Handbook of Fuel Cells: Fundamentals, Technology and Applications", Vol. 3, W. Vielstich, A. Lamm, and H. A. Gasteiger, Editors, John Wiley & Sons, New York, 2003, p. 517.
[3] M. Uchida, Y. Aoyama, N. Eda, A. Ohta, J. Electrochem. Soc. 142 (1995) 4143.
[4] T. V. Reshetenko, J. St-Pierre, J. Electrochem. Soc. 161 (2014) F1089.
[5] J. St-Pierre, B. Wetton, G.-S. Kim, K. Promislow, J. Electrochem. Soc. 154 (2007) B186.
[6] T.V. Reshetenko, G. Bender, K. Bethune, R. Rocheleau, Electrochim. Acta 56 (2011) 8700.
[7] N. Nonoyama, S. Okazaki, A. Z. Weber, Y. Ikogi, T. Yoshida, J. Electrochem. Soc. 158 (2011) B416.
[8] U. Beuscher, J. Electrochem. Soc. 153 (2006) A1788.
[9] J. Stumper, H. Haas, A. Granados, J. Electrochem. Soc. 152 (2005) A837.
[10] D.R. Baker, D.A. Caulk, K.C. Neyerlin, M.W. Murphy, J. Electrochem. Soc. 156 (2009) B991.
[11] K. Sakai, K. Sato, T. Mashio, A. Ohma, K. Yamaguchi, K. Shinohara, ECS Trans. 25 (2009) 1193.
[12] S. Arisetty, X. Wang, R. K. Ahluwalia, R. Mukundan, R. Borup, J. Davey, D. Langlois, F. Gambini, O. Polevaya, S. Blanchet, J. Electrochem. Soc. 159 (2012) B455.
[13] T. Reshetenko, A. Kulikovsky, J. Electrochem. Soc. 163 (2016) F1100.
[14] M. Eikerling, A. A. Kornyshev, J. Electroanal. Chem. 475 (1999) 107.
[15] A.A. Kulikovsky, Electrochimica Acta 55 (2010) 6391.
[16] J.S. Newman, C. W. Tobias, J. Electrochem. Soc. 109 (1962) 1183.
[17] T. Reshetenko, A. Kulikovsky, J. Electrochem. Soc. 164 (2017) E3016.
[18] T. Reshetenko, A. Kulikovsky, J. Electrochem. Soc. 163 (2016) F238.
[19] T. Reshetenko, A. Kulikovsky, J. Electrochem. Soc. 164 (2017) F1633.
[20] T. Reshetenko, A. Kulikovsky, J. Electrochemical Soc. 166 (2019) F1253.
[21] T. Reshetenko, A. Kulikovsky, RSC Advances 9 (2019) 38797
[22] J. St-Pierre, T.V. Reshetenko, ECS Trans., 75 (14) (2016) 63.
[23] T. Reshetenko, G. Bender, K. Bethune, R. Rocheleau, Electrochim. Acta 69 (2012) 220.
[24] K. Broka, P. Ekdunge, J. Appl. Electrochem. 27 (1997) 117.
[25] A.Z. Weber, J. Newman, J. Electrochem. Soc. 152 (2005) A677.
[26] J.H. Nam, M. Kaviany, Int. J. Heat Mass Transfer 46 (2003) 4595.
[27] T. Mashio, A. Ohma, S. Yamamoto, K. Shinohara, ECS Trans. 11 (2007) 529.

[28] Z.H. Wan, Q. Zhong, S.F. Liu, A.P. jin, Y.N. Chen, J.T. Tan, M. Pan, Int. J. Energy Res. 42 (2018) 2225.
[29] M. Debe, J. Electrochem. Soc. 160 (2013) F522.
[30] Y. Ono, T. Mashio, S. Takaichi, A. Ohma, H. Kanesaka, K. Shinohara, ECS Trans. 28 (2010) 69.
[31] T. Greszler, D. Caulk P. Sinha, J. Electrochem. Soc. 159 (2012) F831.
[32] J.P. Owejan, J.E. Owejan, W. Gu, J. Electrochem. Soc. 160 (2013) F824.
[33] P.K. Sinha, W. Gu, A. Kongkanand, E. Thompson, J. Electrochem. Soc. 158 (2011) B831.
[34] F.B. Spingler, A. Phillips, T. Schuler, M.C. Tucker, A.Z. Weber, Int. J. Hydrogen Energy 42 (2017) 13960.
[35] T. Schuler, A. Chowdhury, A.T. Freiberg, B. Sneed, F.B. Spingler, M.C. Tucker, K.L. More, C.J. Radke, A.Z. Weber, J. Electrochem. Soc. 166 (2019) F3020.
[36] R. Halseid, R. Tunold, J. Electrochem. Soc. 153 (2006) A2319.
[37] R.B. Bird, W.E. Stewart, E.N. Lightfoot, "Transport phenomena", 2^{d} edition, John Wiley and Sons, New York, 2002, pp. 513-542.